Stony Brook University

Forward Analysis of Transversely Isotropic Thin Film by Indentation Method

A Thesis Presented

by

Zheng Zhi

to

The Graduate School

in Partial Fulfillment of the

Requirements

for the Degree of

Master of Science

in

Materials Sciences and Engineering

Stony Brook University

May 2013

Stony Brook University
The Graduate School

Zheng Zhi

We, the thesis committee for the above candidate for the
Master of Science degree, hereby recommend
acceptance of this thesis.

Dr. T.A. Venkatesh – Thesis Advisor
Assistant Professor, Materials Science and Engineering

Dr. Tadanori Koga – Second Reader
Associate Professor, Materials Science and Engineering

Dr. Balaji Raghothamachar – Third Reader
Research Assistant Professor, Materials Science and Engineering

This thesis is accepted by the Graduate School

Charles Taber
Interim Dean of the Graduate School

Abstract of the Thesis

Forward Analysis of Transversely Isotropic Thin Film by Indentation Method

by

Zheng Zhi

Master of Science

in

Materials Science and Engineering

Stony Brook University

2012

Instrument indentation based methods for determining elasto-plastic properties of bulk specimen or thin film have received considerable and continue growing attention for recent decades, due to its simplicity, operability, and potential applications. However, the researches of transversely isotropic thin film are still at the beginning stage. In order to obtain a deeper understand of the relationship between $P-h$ curve and thin film properties, both dimensional analysis method and finite element method were applied in the present work. Extensive computational analysis of 630 sets of materials properties was carried out here. Through systematical studies, a more reasonable and intrinsic relationship, between indenter displacement h and the force P on it, was revealed. Also, an effect of materials transverse isotropic properties was summarized. Moreover, accurate and powerful forward analysis functions were established at the end of this thesis. These functions were, then, tested and mismatches were studied.

Dedication To

My Family

Table of Contents

List of Figures

List of Tables

Acknowledgments

Graduate experience at Stony Brook University is one of the most precious wealth of my life. Here, I have met a lot of enthusiasm and talented students, but also known many knowledgeable, high-minded professors and scholars. They gave me a tremendous help in the growth of my life, thought and academic.

First, I would like to thank my thesis advisor, Prof. T.A. Venkatesh for giving me the great chance to come into contact with this field, and letting me to use the resources of our laboratory. Well worth mentioning that during this period, he, with great patience and carefulness, gave me lots of guidance and encouragement.

Furthermore, I would like to thank Dr. Guang Cheng for guiding me patiently how to use the software of ABAQUS. Without his help, it's almost impossible for me to get so many desired results in such a short period. Another doctoral candidate who gave me great help in my research is Hongxu Liu, coming from the department of applied mathematics. From the discussions with him, I have gotten a deeper and basic understanding of some theories and models.

Also, I would like to thank my roommates and classmates like, Xiongfei Wei, Lizhou Nie, Peng Li, Fengzhou He and so on. I'm sorry that I cannot mention the name of each person, but I sincerely appreciate every single help from every single person, and will keep it in my mind forever.

Additionally, I would like to thank my best friends. Whenever I am lost or homesick, it's their encouragement and backing made me to persevere.

Finally, I would like to thank my girlfriend, Fei Wang and my family members for trusting and supporting me all the way.

Give my best wishes to all the people I care about above.

1 Introduction

1.1. Background on instrument indentation

Instrument indentation based methods for determining elasto-plastic properties of bulk specimen or thin film have received considerable and continue growing attention for recent decades, due to its simplicity, operability, and potential applications [1-3]. With the development of science and technology, as well due to the needs of human life, materials from macro to micro, even to nano scales, have been applied widely. The performance of these materials vary significantly while their size changes. In order to characterize these properties in small scales quickly, instrumented indentation analysis, which is derived from the traditional method of hardness testing, is developed to provide an easy, convenient and accurate way.

In almost all indentation studies, problems are solved by trying to get enough information from the $\mathrm{P}-\mathrm{h}$ curve, as in Fig.1-1, where 'P' represents force applied on the indenter, 'h' is the displacement of indenter and 'S' is the slope of the unload curve. Oliver and Phar [4], by applying Sneddon's analysis [5], made an epoch-making and breakthrough in this area, by which elastic property can be obtained from equation as:

$$\mathrm{S} = 2E_r a = \frac{2}{\sqrt{\pi}} E_r \sqrt{A}; \qquad \text{Eq 1-1}$$

Where, a is the contact radius, A is the contact area, and the effective elastic modulus E_r could be expressed as:

$$\frac{1}{E_r} = \frac{1-\nu^2}{E} + \frac{1-\nu_i^2}{E_i}; \qquad \text{Eq 1-2}$$

Here, the subscripts 'i' represented indenter. They also got good results for deterring the hardness of bulk specimen with above method [6]. However, such way is restrict to the condition when contact edge of bulk specimen is sink-in, while for lots of materials, the edge is pile-up [7].

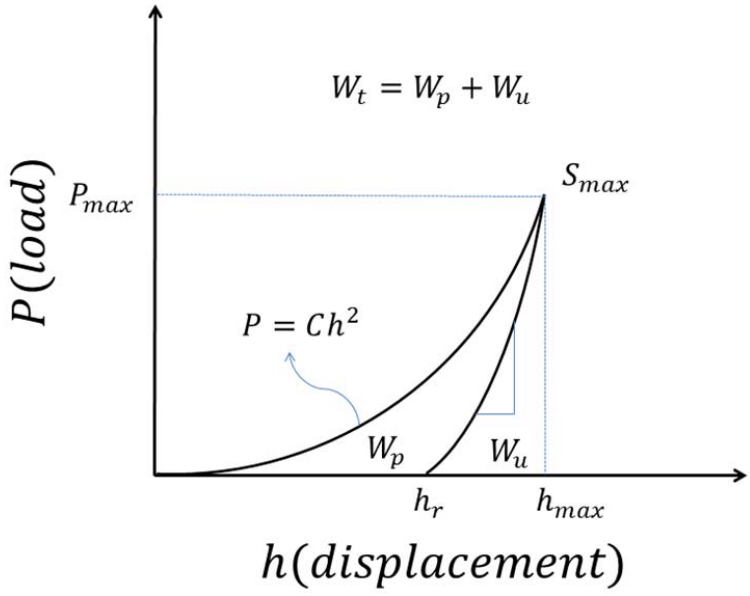

Figure 1-1: Schematic diagram of instrumented indentation P-h curve.

Dao [8], Cheng and Cheng [9, 10] pioneered and perfected the numerical method, by applying scaling laws and dimensional analysis, which is still a mainstream and powerful method today. During this period, Venkatesh et al [2] proposed the idea of forward and reverse analysis, which had become a fixed process of instrument indentation research either for simulations only or for simulations accompanied experiments (Fig.1-2). Instrument indentation method can, not only, been used to get the elastic and plastic properties from $\mathrm{P}-\mathrm{h}$ curve of indenting specimens [11, 12], but also can help to learn the deformation, fatigue, creep, fail behaviors of materials [13-18]. Moreover, this method is not restrict in the area of engineering, it has been adopted in many other field like geology[19], biomedical[20], marine biology[21] etc. In a word, instrumented indentation method is a maturing technology can be widely applied.

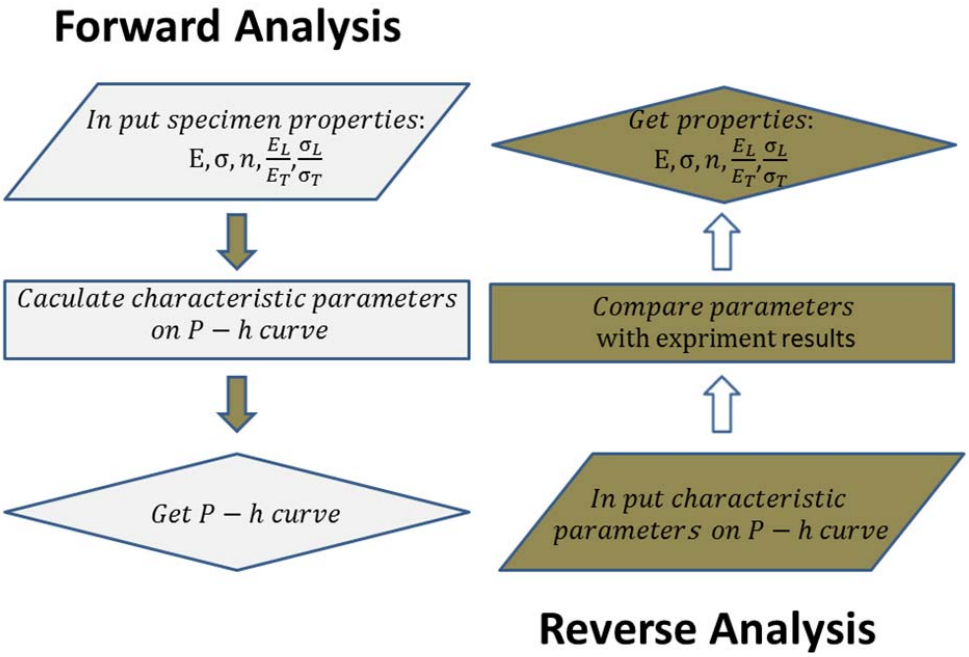

Figure 1-2: Schematic diagram of the process of forward and reverse analysis.

1.2. Transversely isotropic materials and instrumented indentation

1.2.1. Definition of transversely isotropic materials

A transversely isotropic material is one with physical properties symmetric about an axis normal to a plane of isotropy which means within this plane, all properties of this material are the same in all directions. In the present paper, the direction perpendicular to the plane of isotropy is defined as longitudinal direction, and the direction parallel to the plane of isotropic is defined as transverse direction.

1.2.2. Elastic properties of transversely isotropic materials

Many thin films and coating might exhibit transversely isotropic property due to their fabrication process and the resulting microstructures [22]. Nakamura et al

proposed that for a transversely isotropic material, there were five independent constants to describe the elastic properties. Furthermore, the compliance matrix of a transversely materials can be represented as:

$$\begin{bmatrix}\varepsilon_{11}\\ \varepsilon_{22}\\ \varepsilon_{33}\\ \gamma_{12}\\ \gamma_{23}\\ \gamma_{13}\end{bmatrix} = \begin{bmatrix} 1/E_T & -\nu_{LT}/E_L & -\nu_T/E_T & 0 & 0 & 0\\ -\nu_{TL}/E_T & 1/E_L & -\nu_{TL}/E_T & 0 & 0 & 0\\ -\nu_T/E_T & -\nu_{LT}/E_L & 1/E_T & 0 & 0 & 0\\ 0 & 0 & 0 & 1/G_L & 0 & 0\\ 0 & 0 & 0 & 0 & 1/G_L & 0\\ 0 & 0 & 0 & 0 & 0 & 1/G_T \end{bmatrix} \begin{bmatrix}\sigma_{11}\\ \sigma_{22}\\ \sigma_{33}\\ \sigma_{12}\\ \sigma_{23}\\ \sigma_{13}\end{bmatrix}; \quad \text{Eq 1-3}$$

Where, the subscripts 'L' and 'T' are, respectively, denoted to directions of longitudinal and transverse. Similarly, subscripts '1' and '3' represented the directions of transverse, while subscript '2' represented the direction of longitudinal, as illustrated in Fig.1-3.

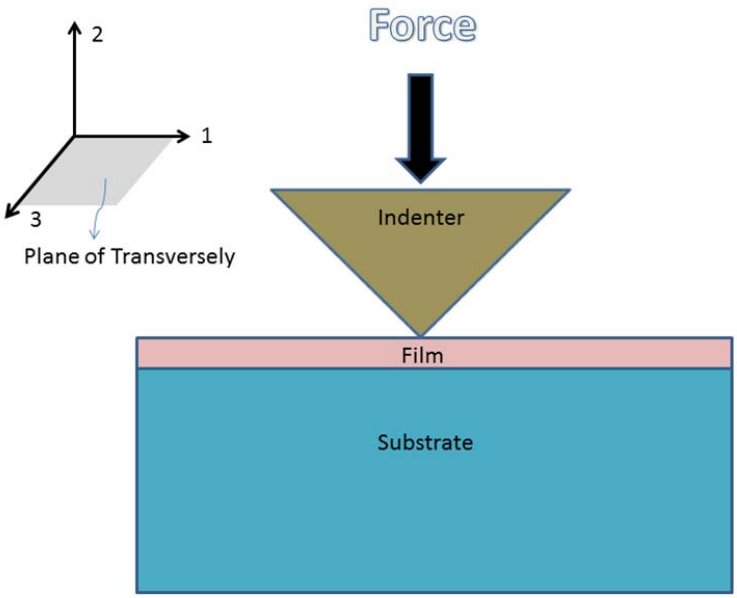

Figure 1-3: Schematic diagram of indentation on transversely isotropic thin film.

The in-plane shear modulus, G_T as:

$$G_T = \frac{E_T}{2(1+\nu_T)}; \quad \text{Eq 1-4}$$

In order to reduce the variables, the out-of-plane, G_L can be approximately expressed as:

$$G_L = \frac{E_0}{2(1+\left(\frac{\nu_L+\nu_T}{2}\right))}; \quad \text{Eq 1-5}$$

Where, E_0 is the average Young's modulus as $(E_T + E_L)/2$.

1.2.3. Plastic properties of transversely isotropic materials

Hill's [23] has developed a yield criterion for anisotropic plastic deformation as:

$$\mathrm{F}(\sigma_{22} - \sigma_{33})^2 + \mathrm{G}(\sigma_{33} - \sigma_{11})^2 + \mathrm{H}(\sigma_{11} - \sigma_{22})^2 + 2\mathrm{L}{\sigma_{23}}^2 + 2\mathrm{M}{\sigma_{31}}^2 + 2\mathrm{N}{\sigma_{12}}^2 = 1 \quad \text{Eq 1-6}$$

Here, $\mathrm{F}, \mathrm{G}, \mathrm{H}, \mathrm{L}, \mathrm{M}, \mathrm{N}$ are constants that have to be determined experimentally

Equation (1-6) can be modified for transversely isotropic materials as [22]:

$$\mathrm{f}(\sigma) = \sqrt{\mathrm{P}(\sigma_{22} - \sigma_{33})^2 + \mathrm{P}(\sigma_{22} - \sigma_{11})^2 + \mathrm{Q}(\sigma_{11} - \sigma_{33})^2 + 2\mathrm{R}{\tau_{23}}^2 + 2\mathrm{R}{\tau_{12}}^2 + 2\mathrm{S}{\tau_{13}}^2} - \sigma_0 = 0; \quad \text{Eq 1-7}$$

Here, $\mathrm{P}, \mathrm{Q}, \mathrm{R}$ and S are the dimensionless constant that related to σ_0 as:

$$\mathrm{P} = \frac{1}{2}\left(\frac{\sigma_0}{\sigma_{0L}}\right)^2; \quad \text{Eq 1-8}$$

$$\mathrm{Q} = \frac{1}{2}\left(2\frac{{\sigma_0}^2}{{\sigma_{0T}}^2} - \frac{{\sigma_0}^2}{{\sigma_{0L}}^2}\right); \quad \text{Eq 1-9}$$

$$\mathrm{R} = \frac{1}{2}\left(\frac{\sigma_0}{\tau_{0L}}\right)^2; \quad \text{Eq 1-10}$$

$$\mathrm{R} = \frac{1}{2}\left(\frac{\sigma_0}{\tau_{0T}}\right)^2; \quad \text{Eq 1-11}$$

Here, σ_0 is the reference stress equal to $(\sigma_{0\mathrm{L}} + \sigma_{0\mathrm{T}})/2$, and $\sigma_{0\mathrm{L}}, \sigma_{0\mathrm{T}}, \tau_{0\mathrm{L}}, \tau_{0\mathrm{L}}$ are yield stressed along different direction respectively. In order to reduce the variables, $\tau_{0\mathrm{L}}, \tau_{0\mathrm{L}}$ can be approximately expressed as:

$$\tau_{0L} = \frac{\sigma_0}{\sqrt{3}}\sqrt{\frac{\sigma_{0L}}{\sigma_{0T}}}; \quad \text{Eq 1-12}$$

$$\tau_{0T} = \frac{\sigma_0}{\sqrt{3}};$$ Eq 1-13

1.2.4. Post yielding Behavior

Lan et al[3] described stress-strain, elasto-plastic behavior of bulk materials as:

$$\sigma = \begin{cases} E\epsilon, (\sigma \leq \sigma_Y) \\ R\epsilon^n = \sigma_Y \left(1 + \frac{E}{\sigma_Y}\epsilon_n\right)^n, (\sigma \geq \sigma_Y) \end{cases};$$ Eq 1-14

Where E is the Young's modulus, n is the strain hardening exponent, σ_Y in the yield stress at initial, and ϵ_n is the non-linear part strain.

To extend the isotropic power law hardening to a transversely isotropic materials, then,

$$\sigma_L = \begin{cases} E\epsilon_L, (\sigma_L \leq \sigma_{0L}) \\ R\epsilon_L^n = \sigma_L \left(1 + \frac{E}{\sigma_{0L}}\epsilon_{nL}\right)^n, (\sigma_L \geq \sigma_{0L}) \end{cases};$$ Eq 1-15

and

$$\sigma_T = \begin{cases} E\epsilon_T, (\sigma_T \leq \sigma_{0T}) \\ R\epsilon_T^n = \sigma_T \left(1 + \frac{E}{\sigma_{0T}}\epsilon_{nT}\right)^n, (\sigma_T \geq \sigma_{0T}) \end{cases};$$ Eq 1-16

1.3. Scaling, dimensional analysis, and instrumented indentation

Two geometric objects are described as geometric similar in their lengths are all proportional to each other with the same proportional constant, and all angles are identical [24]. For indentation test, due to introducing of length parameter of displacement of indenter, sphere and flat cylinder indenter are not geometric similar anymore if radii are not equal. However for cone indenter, if half angles are equal, then, all cone indenters are geometric similar.

The so-called Π-theorem, which was proposed by Buckingham[25], is the basic idea of dimensional analysis, which emphasized that physical laws do not depend on arbitrarily chosen basic units of measurement, or to say that all the items that are added together must have the same unit. In indentation, two basic dimensions are L and M. And all unknown amount could be, without loss of generality, written as:

$$\mathrm{y} = \mathrm{f}(x_1, x_2, \cdots, x_n); \qquad \text{Eq 1-17}$$

And assume that x_1 and x_2 have independent dimensions, so:

$$\mathrm{y}/({x_1}^{a1} \times {x_2}^{a2}) = \mathrm{F}(x_1, x_2, \frac{x_3}{{x_1}^{a_{31}} \times {x_2}^{a_{32}}} \cdots, \frac{x_n}{{x_1}^{a_{n1}} \times {x_2}^{a_{n2}}}); \qquad \text{Eq 1-18}$$

where $\mathrm{y}/({x_1}^{a1} \times {x_2}^{a2})$ and $\frac{x_n}{{x_1}^{a_{n1}} \times {x_2}^{a_{n2}}}$ are all dimensionless items. Since physical laws do not depend on arbitrarily chosen basic units of measurement, then:

$$\mathrm{y}/({x_1}^{a1} \times {x_2}^{a2}) = \Pi(\frac{x_3}{{x_1}^{a_{31}} \times {x_2}^{a_{32}}} \cdots, \frac{x_n}{{x_1}^{a_{n1}} \times {x_2}^{a_{n2}}}); \qquad \text{Eq 1-19}$$

It's obviously that by applying Π-theorem, numbers of variables in instrument indentation could be reduced by two. Also several important conclusions, which might explain some phenomena, could be obtained directly for dimension analysis, as show in later chapters. To facilitate the successful application, 3 main steps are listed as: [24]

1. Listing all in dependent variables those dependent variables, i.e. the parameters with quantity of interest.

2. Identifying independent variables and parameters with independent dimensions.

3. Forming dimensionless quantities and creating Π functions.

Of course, there are other details should be cared about which would also be seen in next chapters.

1.4. Framework for the indentation analysis of transversely isotropic thin films

The main object of this work is to develop a computational tool for the forward analysis of transversely isotropic thin film on the substrate with already known properties, while all indentations are along the longitudinal direction. Both dimensional analysis and finite element method (FEM) are applied to establish the relationships between indentation responses, i.e. $P-h$ curve, and elastic & plastic properties of materials of thin film. Next parts of this thesis are organized as follows:

Chapter 2 Details of Finite element analysis

Chapter 3 Results discussions and establishment of forward analysis functions

Chapter 4 Conclusions and prospects

2 Finite element analysis

The FEM simulations are carried out by using general purpose finite element package of ABAQUS on DELL workstation T7500. For indentation alone longitudinal direction, it's convenient and practical to take advantage of the axisymmetric property of the thin film. The thickness of thin film, δ, is as 2μm. The total width and height of model are as larger 3000 times as the thickness of the film, in order to diminish the effect of the bottom boundary (Fig.2-1). The cone indenter is modeled by rigid surface with half apex angle of $70.3°$. And the assumption of no friction between indenter and film is applied due to that friction is a minor factor here [26]. Totally 20000 elements, mixed of CAX4R and CAX3 are used to mesh both film and substrate, shown in (Fig.2-2).

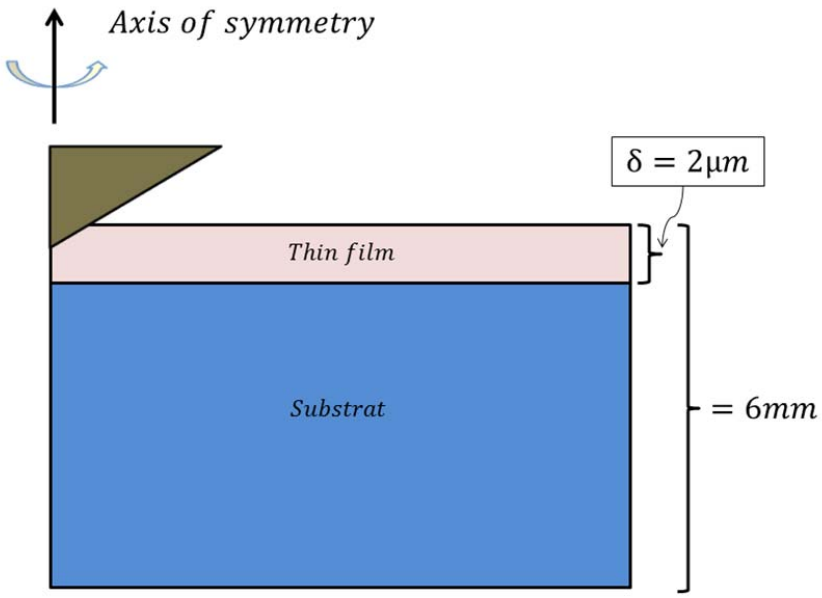

Figure 2-1: Schematic diagram of 2-D axisymmetric simulation models

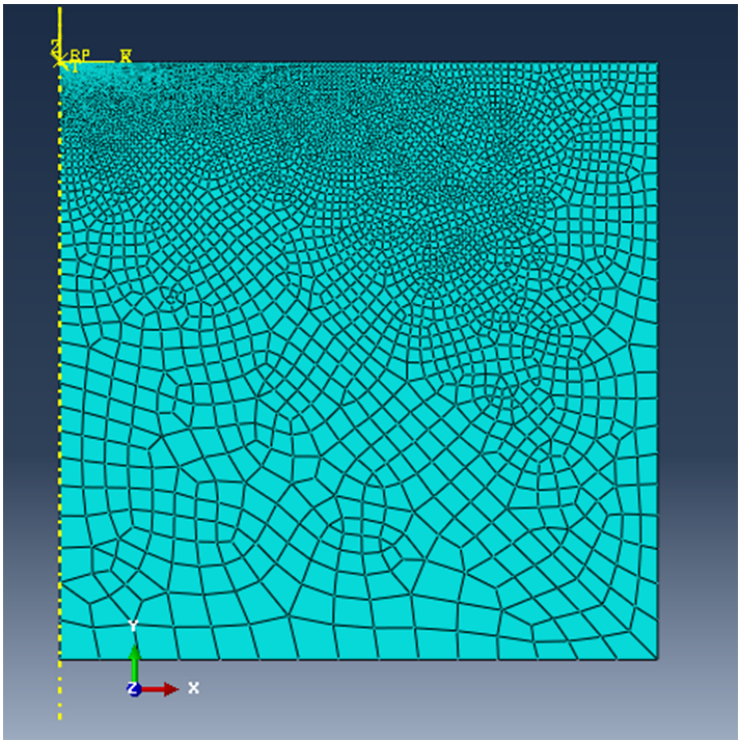

Figure 2-2: Schematic diagram of mesh on specimen

3 Results and discussions

3.1. Relationship between indenter displacement and the force on it

Sneddon derived a general relationship among the displacement of indenter, h, and the loading load of indenter, P, for a solid punch that could be described as revolution of a smooth function into a bulk material, as below[5]:

$$\mathrm{P} = \mathrm{C}h^{m}; \qquad \text{Eq 3-1}$$

where C is the loading curvature for a certain kind of material and a certain kind of punch, and m is a constant for a certain kind geometric of punch, i.e. $\mathrm{m} = 2$ for cones, $\mathrm{m} = 1.5$ for spheres and paraboloids of revolution, and $\mathrm{m} = 1$ for flat cylinders. Prerequisite for the establishment of this relationship is that deformations were limited to elastic. With advanced studies, Oliver and Pharr found this relationship still kept for cone indenter [4], however, exponent m was no longer a fixed value for sphere punches with different radius [27], when considering plastic deformation.

These phenomena could be well explained by scaling laws and dimensional analysis [24]. In which, load P is dependent on variables as $E, v, \sigma_Y, n, h, \theta$, for a rigid cone indenter, that is:

$$\mathrm{P} = \mathrm{P}(E, v, \sigma_Y, n, h, \theta); \qquad \text{Eq 3-2}$$

where E represents Young's modulus, σ_Y represents yield stress, v represents Poisson's ration, n represents strain hardening exponent, and θ is the half angle of cone indenter. By applying the dimensional analysis, equation (3-2) become:

$$\mathrm{P} = \sigma_Y h^2 \Pi_a \left(\frac{E}{\sigma_Y}, v, n, \theta\right); \qquad \text{Eq 3-3}$$

Since there is no other length parameter in the expression of Π_a, then there of course have no items related to h in Π_a, so the force on the indenter, P , is just proportional to the square of the indenter displacement, h, regardless of properties of bulk materials.

For a sphere indenter, P is additionally dependent on the radius of the indenter, r, that is:

$$\mathrm{P} = \mathrm{P}(E, v, \sigma_Y, n, h, \theta, r); \qquad \text{Eq 3-4}$$

alternatively, equation (3-4) is equal to:

$$\mathrm{P} = \sigma_Y h^2 \Pi_b \left(\frac{E}{\sigma_Y}, v, n, \theta, \frac{r}{h}\right); \qquad \text{Eq 3-5}$$

Since Π_b contains item r/h , it's obviously P is never more proportional to the square of h, but actually proportional to $h^{1.5}$ under the limit of elastic deformation (i.e., $\sigma_Y \to \infty$), and the exponent even deviate from 1.5 when σ_Y is introduced.

Based on the analysis above, it seems safety to make a prediction that loading load P is no longer proportional to h for a flat-tip cylinder indenter, when the deformation is not restricted to elastic which has been proved by the FEM and show in (Fig. 3-1).

In this work, we concern the situation when cone indenter ($\theta = 70.3°$) punch into thin film on a substrate with different properties. Due to the presenting of the secondary kind of material, relationship between displacement, h, and load, P becomes more complex. Zhao et al. [28] proposed that it was possible to assume the $\mathrm{P} - h$ curve of a film indentation experiment as:

$$\mathrm{P} = C_0 h^{m(h/\delta)}; \qquad \text{Eq 3-6}$$

where δ is the thickness of the film and C_0 is the loading curvature obtained from bulk specimen of the film. Here exponent m become a function of the normalized penetration. Also, one could fit the curve by:

$$\mathrm{P} = \mathrm{C}(\mathrm{h}/\delta)h^2; \qquad \text{Eq 3-7}$$

where the exponent is fixed at the value of two just as the bulk materials test, while the curvature become a function of the normalized penetration.

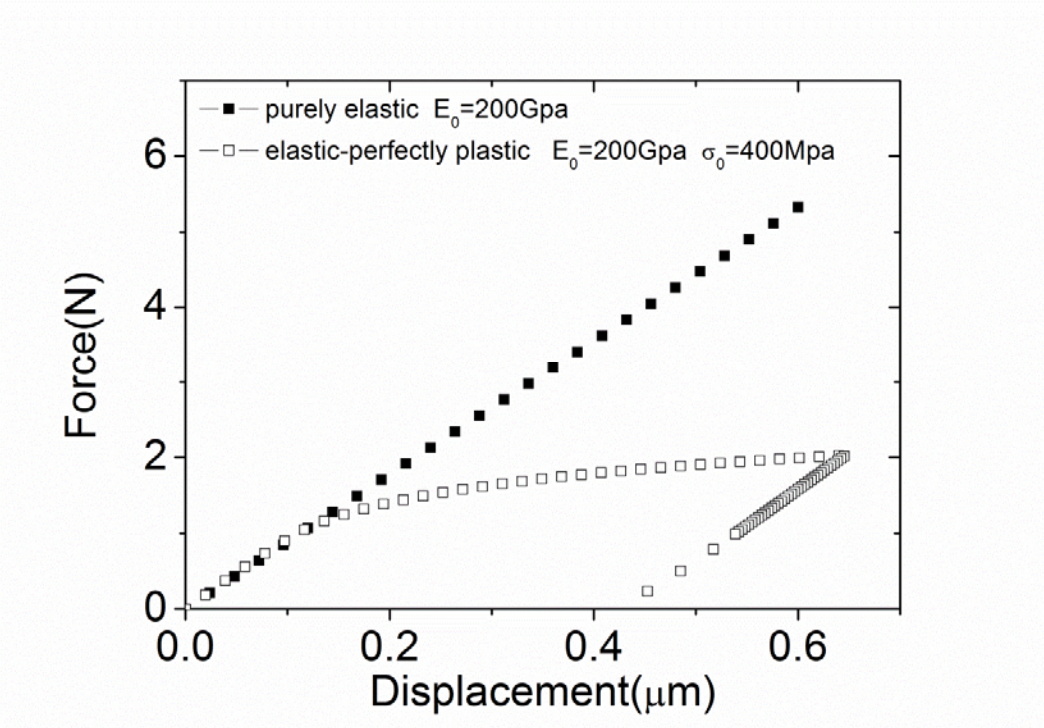

Figure 3-1: A comparison of dissimilar responses when flat-tip indenter punching into homogeneous, isotropic semi-infinite bulk specimens with varying property.

Alternatively, to keep the generality, one could fit the loading curve with both C and m varying with h/δ as:

$$\mathrm{P} = \mathrm{C}(\mathrm{h}/\delta)h^{m(h/\delta)}; \qquad \text{Eq 3-8}$$

Zhao et al. [28] discovered the load curvature increasing with h/δ, where $\mathrm{C}(0) = C_0$, when using equation (3-7) as the fitting function.

With future research by FEM, the results displayed that the load curvature C is always gradually shifting from C_0 to C_s (Fig. 3-2), which means that curvature might increase, but was also possible to reduce. The film's properties were fixed with $E_0 = 150\mathrm{Gpa}$, $\sigma_0 = 400\mathrm{Mpa}$ and $\mathrm{n} = 1$ (here, C_0 =0.0371N/μm^2, C_s is the load curvature of substrate in bulk indentation test, Table 3-1).

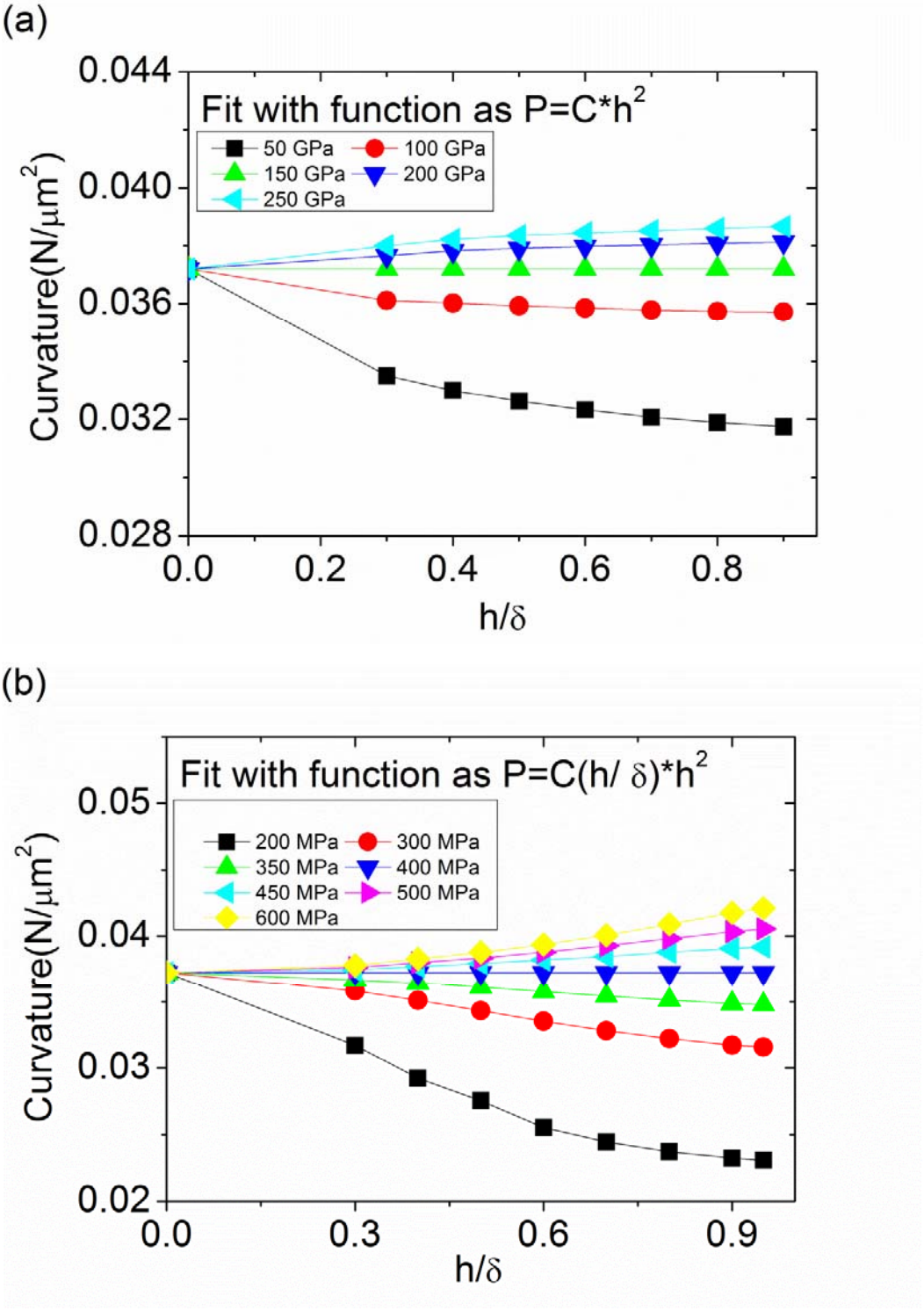

Figure 3-2: Loading curvature shifts from C_0 to C_s when penetration displacement gradually increases, with fixed properties of the thin film, accompanied by varying properties of substrate: for (a) $\sigma_s = 400\text{Mpa}$, E_0/E_svarying from $1/3$ to $5/3$, $n_S = 1$; for (b) $E_s = 150\text{GPa}$, σ_0/σ_svarying from $1/2$ to $3/2$, $n_S = 1$.

Table 3-1: Load curvature C_s for substrate with different properties

For $1/3 \leq E_0/E_s \leq 5/3$			For $1/2 \leq \sigma_0/\sigma_s \leq 3/2$		
E_s(GPa)	σ_s(MPa)	C_s(N/μm2)	E_s(GPa)	σ_s(MPa)	C_s(N/μm2)
N/A	N/A	N/A	150	200	0.01605
50	400	0.02686	150	300	0.02725
100	400	0.03296	150	350	0.03154
150	400	0.03560	150	400	0.03560
200	400	0.03707	150	450	0.03970
250	400	0.03763	150	500	0.04365
N/A	N/A	N/A	150	600	0.05115

Zhao et al. [28] proposed the entire curvature of $\mathrm{P}-h$ curve was constantly increase might due to they set substrate as rigid body when doing simulations.

Zhao and Chen [29] altered to adopt equation (3-6), and proposed that exponent m is affected by substrate and does not equal to 2 even when $E_0/E_s = 1$. In present work, with future research by FEM, the results shows that exponent m does not only deviate from the value of 2, but also continuously varying by the increment the displacement, h. Fig.3-3 indicates that if the film is "harder" than the substrate (i.e. $E_0/E_s > 1$ and $\sigma_0/\sigma_s > 1$), exponent m tend to firstly decrease to a small value, and then increase back to 2 at some point. On the contrary, if the film is "softer" than the substrate (i.e. $E_0/E_s < 1$ and $\sigma_0/\sigma_s < 1$), m will initially increase, and then drop back to 2. All dates in Fig.3-3 were obtained by assuming the substrate properties as elastic-perfect plastic, i.e. $n_s = 0$.

(a)

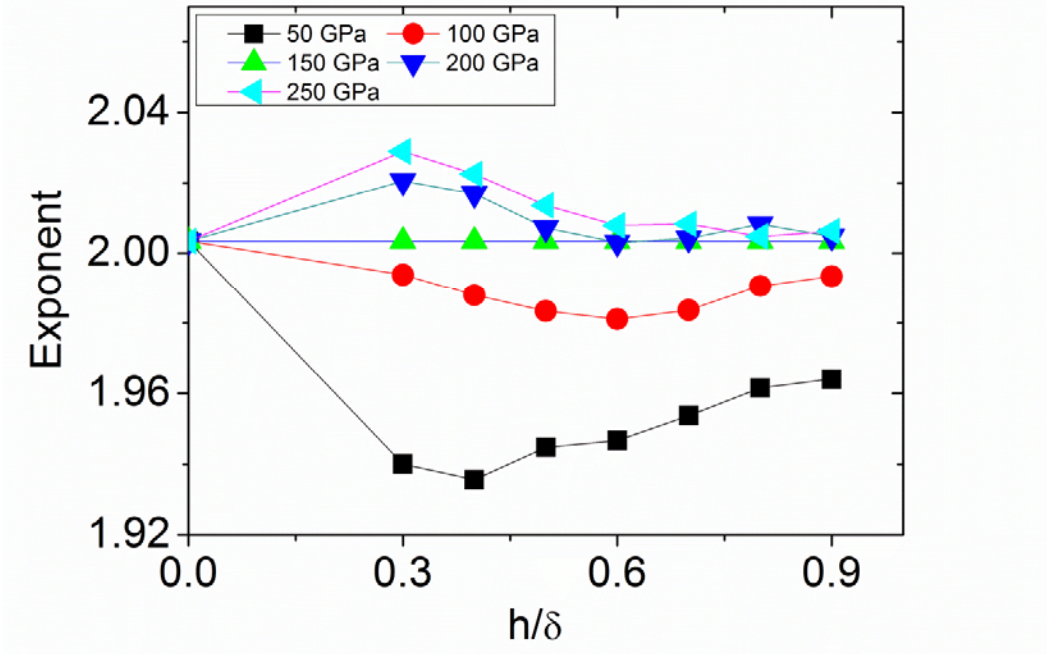
50 GPa
100 GPa
150 GPa
200 GPa
250 GPa
Exponent
2.04
2.00
1.96
1.92
0.0
0.3
0.6
0.9
h/δ

(b)

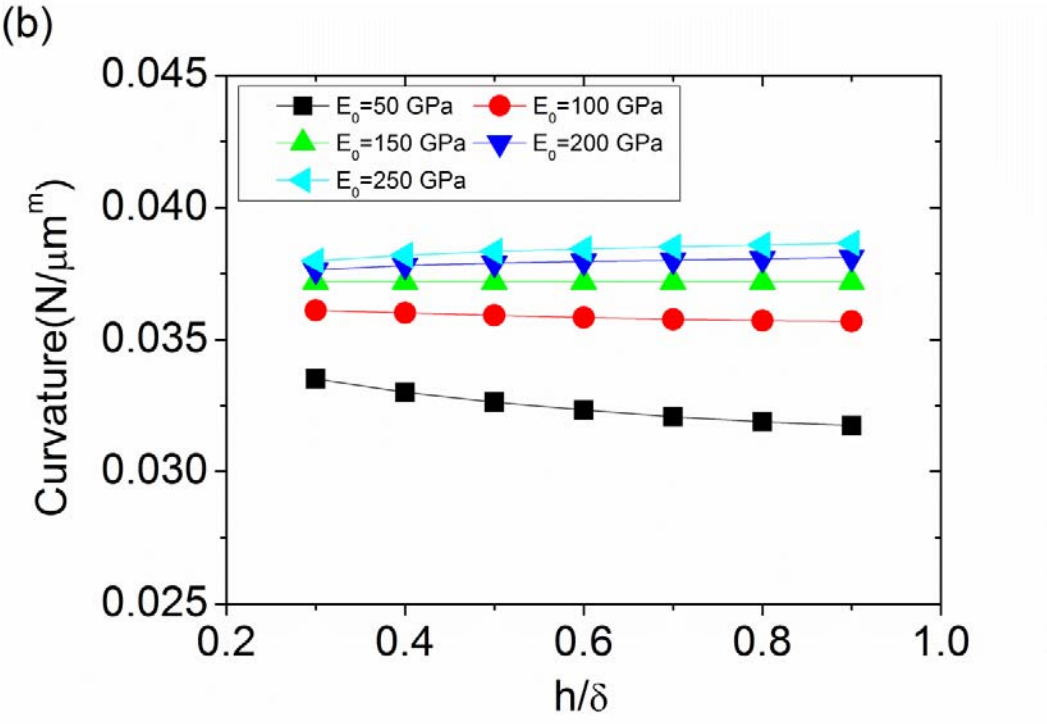
E0=50 GPa
E0=100 GPa
E0=150 GPa
E0=200 GPa
E0=250 GPa
Curvature(N/μm^m)
0.045
0.040
0.035
0.030
0.025
0.2
0.4
0.6
0.8
1.0
h/δ

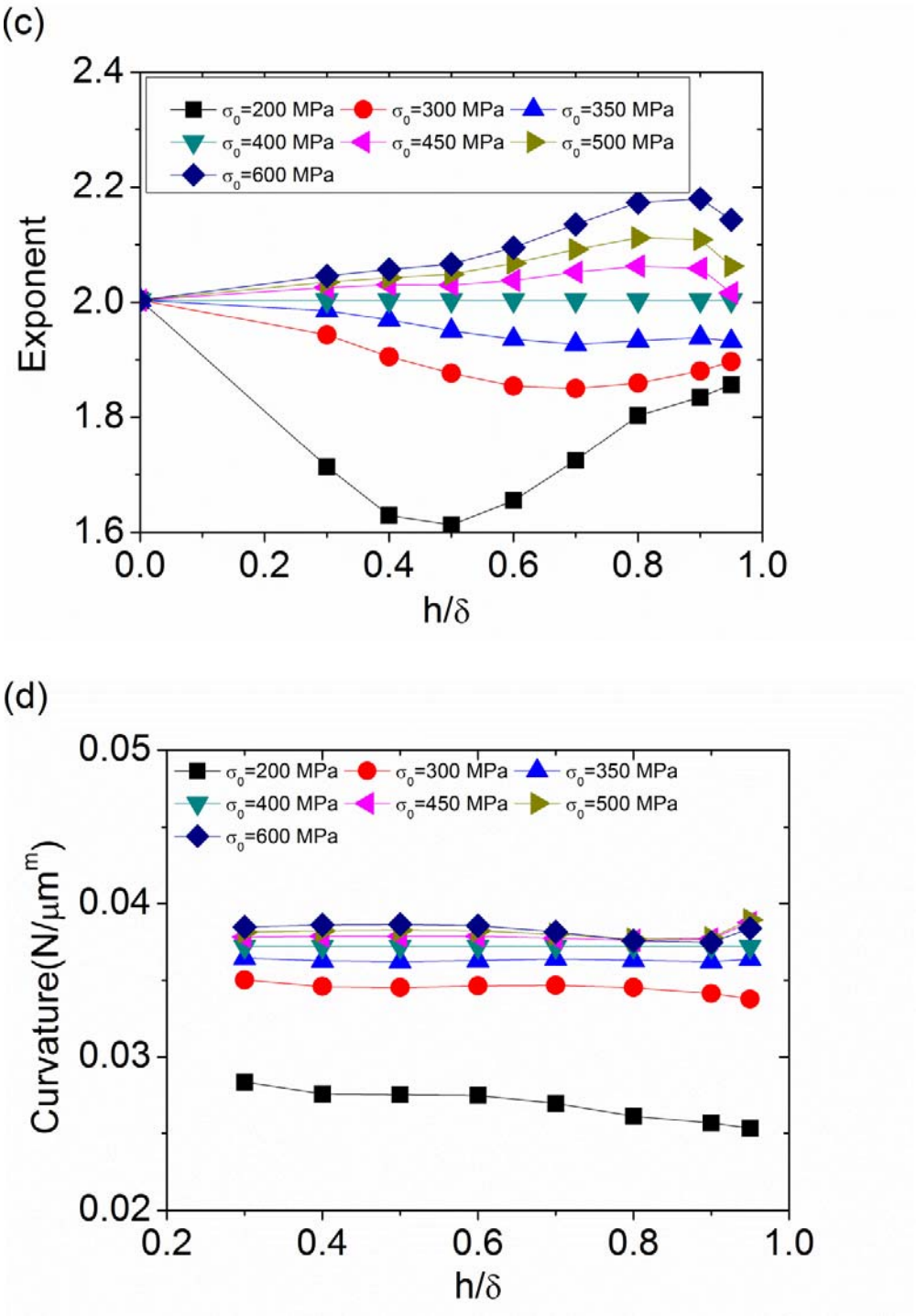

Figure 3-3: Fitting $\mathrm{P}-\mathrm{h}$ curve with function $\mathrm{P}=\mathrm{C}(\mathrm{h}/\delta)\mathrm{h}^{\mathrm{m}(\mathrm{h}/\delta)}$ to get the values of both exponent m and curvature C, when properties of film is fixed, i.e. $E_0 = 150GPa$, $\sigma_0 = 400\mathrm{MPa}$: for (a) and (b) $\sigma_s = 400\mathrm{Mpa}$, E_0/E_s varying from $1/3$ to $5/3$; for (c) and (d) $E_s = 150\mathrm{GPa}$, σ_0/σ_s varying from $1/2$ to $3/2$.

These phenomena probably due to the stress distribution in the film and the substrate, in the early stage of the indentation formed, was very discordant. But with the indentation depth increases, between the film and the substrate, to the extent that mismatch of stress distribution could affect the overall stress distribution was getting smaller and smaller, so m again returned to a value of 2. Moreover, while the film is "soft" (i.e. while E_0 and σ_0 are small), changes in film's properties could affect $\mathrm{P}-\mathrm{h}$ curve significantly. All these dates in Fig.3-3 were obtained through fitting the curve section by section (e.g. fitting date through $\mathrm{h}/\delta=0.3$ to $\mathrm{h}/\delta=0.5$ to found the value of m at point of $\mathrm{h}/\delta=0.4$). It is because that, by such method curve's characteristics could be preserved. More interesting, throughout the whole process of penetration, curvature C practically retains a constant equal to the average of C_0 and C_s which calls up another possible fitting expression of $\mathrm{P}-\mathrm{h}$ curve:

$$\mathrm{P}=\frac{\mathrm{C}_0+\mathrm{C}_\mathrm{s}}{2}\mathrm{h}^{\mathrm{m}(\mathrm{h}/\delta)}; \qquad \text{Eq 3-9}$$

Through extensive simulations analysis, it's clearly both equations (3-9) and (3-8) reveal better conformity than equation (3-7) and (3-6). In present paper, in order not to be loss of generality, equation (3-9) would be adopted next. Another important conclusion obtained here from comparing (Fig.3-2) and (Fig.3-3) is that, plasticity affects the $\mathrm{P}-h$ curve greater than elasticity (which agrees with the results in following sections when property anisotropy is introduced).

Since there is a minimum and maximum value of exponent m during the penetration process, it hopes that there would also be some evidence emerging on the $\mathrm{P}-h$ curve near these points. With a detailed simulation, in Fig.3-4, dramatic ups and downs appear on the $\mathrm{P}-h$ curve when the film is 'hard' than the substrate, with the position of which directly correspond to the position of the minimum value m, which as well indicating that the section by section fitting method is reasonable and effective.

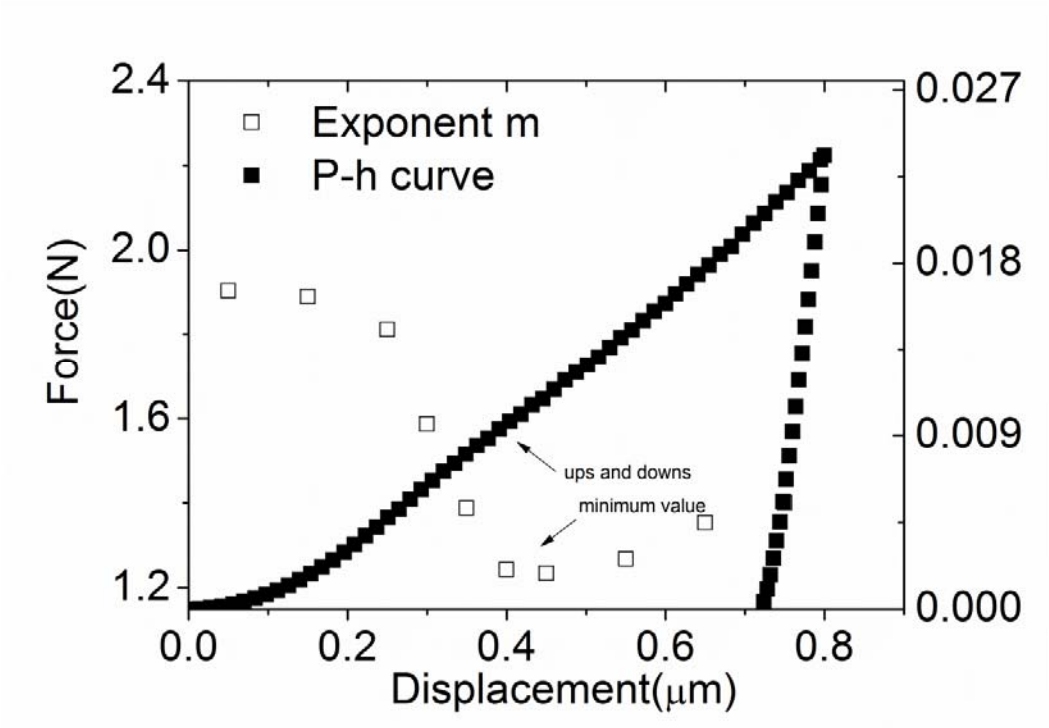

Figure 3-4: Schematic of dramatic ups and downs on $\mathrm{P}-\mathrm{h}$ curve obtained by punching indenter into a specimen with topper film properties set as $E_0 = 200\mathrm{GPa}$, $\sigma_0 = 1000\mathrm{MPa}$ and $\mathrm{n}_0 = 1$, and substrate properties were $E_S = 50\mathrm{GPa}$, $\sigma_S = 200\mathrm{MPa}$ and $\mathrm{n_S} = 1$. Meanwhile, trend of exponent m was also included to see the intrinsic connection between these two curves.

The deviation of m from value 2 for indenter punching into thin films can be similarly explained by dimensional analysis as before:

$$\mathrm{P} = \mathrm{P}(E_0, E_S, v_0, v_s, \sigma_0, \sigma_s, n_0, n_s, h, \delta, \theta); \qquad \text{Eq 3-10}$$

applying the Π theorem, equation (3-10) turns to:

$$\mathrm{P} = \sigma_{Y0} h^2 \Pi_c \left(\frac{E_0}{\sigma_0}, \frac{E_S}{\sigma_0}, v_0, v_s, \frac{\sigma_s}{\sigma_0}, n_0, n_s, \frac{\delta}{h}, \theta\right); \qquad \text{Eq 3-11}$$

Since there is an item (i.e. δ/h) contains length variable h, it's not surprise that exponent m deviates from 2 for thin film instrumented indentation.

3.2. Instrument indentation for transversely isotropic thin film

3.2.1. Necessary assumptions and the properties selecting before simulations

When taking into account the anisotropy of the materials, the situation becomes extremely complex, because too many variables can affect $\mathrm{P}-h$ curve. Limited to the time consumption and computational efficiency, five assumptions are first presented here:

(a) Properties of substrate are already known before indentation;

(b) Anisotropic materials here refer only to transversely isotropic materials;

(c) Only longitudinal indentations (i.e. indentations are perpendicular to the plane of isotropy) are simulated at this point.

(d) All materials tested are elastic-perfect plastic (i.e. $n_0 = 0$)

(e) Indenter is assumed to be rigid body (i.e. $E_r = E_0$)

Totally 630 sets of parameters were conducted here. These cases represented common engineering metals: that is, Young's modulus E_0 ranged from 50GPa to 250GPa, yield strength σ_0 from 200Mpa to 1000Mpa, elastic anisotropy ratio from 1.0 to 1.5, plastic anisotropy ratio from 1.0 to 1.5, and Poisson's ratio v_0 was fixed at 0.3 through all simulation. A more intuitive combination way is show in Fig.3-5. Al-6092-17.5-SiC-whiskers (i.e. $E_S = 121Gpa$, $E_L/E_T = 1.05$, $\sigma_S = 452.5Mpa$, $\sigma_{0L}/\sigma_{0T} = 1.15$, $n_S = 0.1$, $v_S = 0.33$)is preferred to be the fixed property material of substrate, not only because it is widely used in engineering, but also because the property values are in a medium range which is benefit for research works.

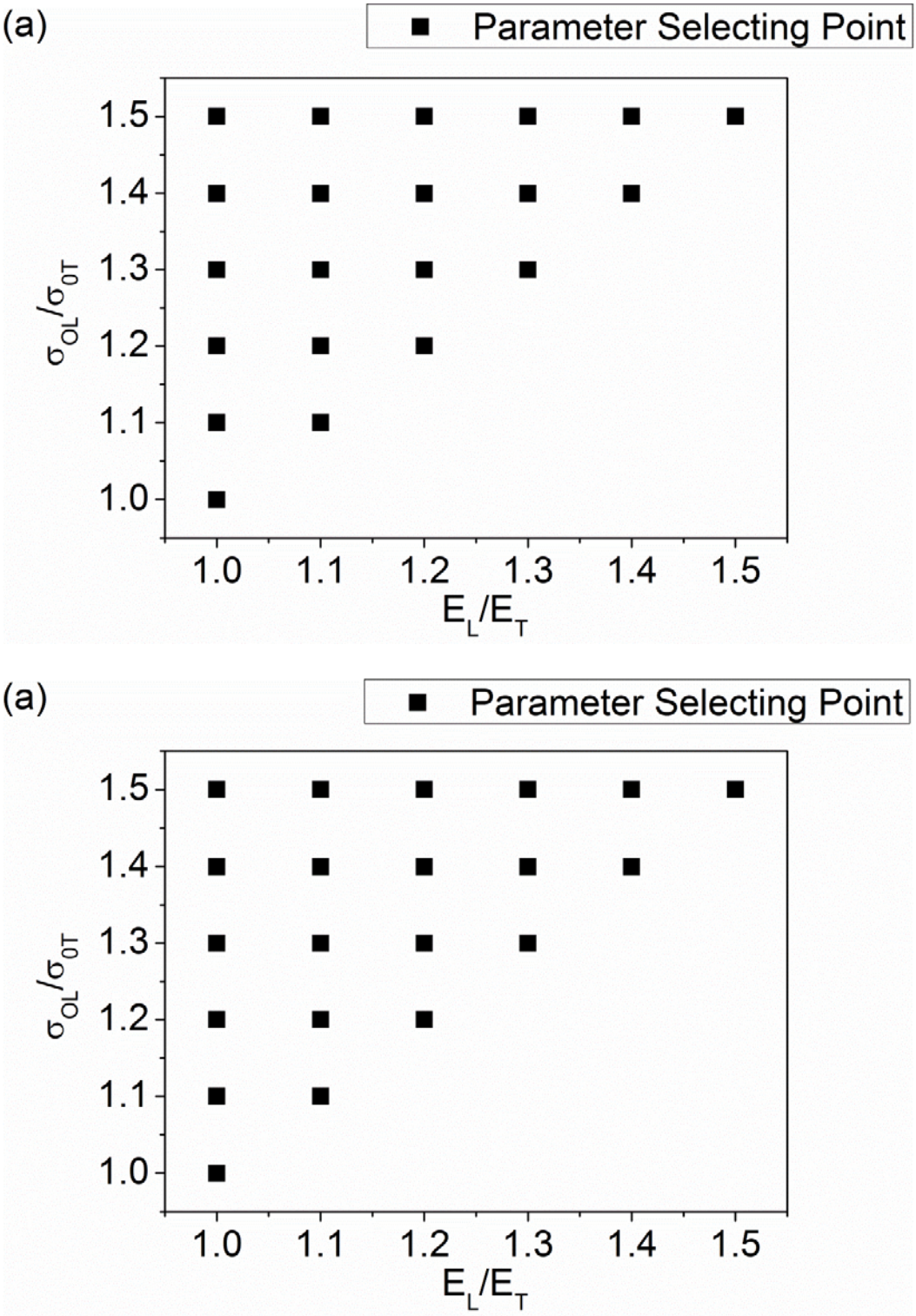

Figure 3-5: Points in (a) and (b) represented thin film properties which have been selected for simulations with variable combinations among $E_0,\ \sigma_0, E_L/\ E_T$ and σ_{0L}/σ_{0T}

3.2.2. Simulations results discussions and analyses

3.2.2.1. Dimension analysis

Based on the five assumptions above, problems are simplified to be dependent on eight variables, namely, E_0, v_0, σ_0, h, δ, θ, E_L/E_T, σ_{0L}/σ_{0T}. Furthermore, as v_0 has little effect on $\mathrm{P}-h$ curve, i.e. negligible, and θ is fixed at 70.3°, then number of variables is reduced to six. In order to understand more about the relationship between P and h, dimensional analysis need to be once again applied, from equation (3-11), we can get:

$$\mathrm{P}=\sigma_0 h^2 \Pi_d\left(\frac{E_0}{E_s},\frac{\sigma_0}{\sigma_s},\frac{h}{\delta},\frac{E_L}{E_T},\frac{\sigma_{0L}}{\sigma_{0T}}\right) \quad \text{Eq 3-12}$$

where, according to assumptions above, E_S and σ_S are already known.

Chen [30] proposes a method of using the impact of substrate to analysis the penetration process. They further put forward three characteristic parameter on $\mathrm{P}-h$ curve, respectively, are

$$\frac{P_e}{\sigma_0 {h_e}^2}=\Pi_e\left(\frac{E_0}{E_s},\frac{\sigma_0}{\sigma_s},\frac{h_e}{\delta},\frac{E_L}{E_T},\frac{\sigma_{0L}}{\sigma_{0T}}\right) \quad \text{Eq 3-13}$$

$$\frac{P_f}{\sigma_0 {h_f}^2}=\Pi_f\left(\frac{E_0}{E_s},\frac{\sigma_0}{\sigma_s},\frac{h_f}{\delta},\frac{E_L}{E_T},\frac{\sigma_{0L}}{\sigma_{0T}}\right) \quad \text{Eq 3-14}$$

$$\frac{W_u}{E_0(h_{max}-h_r)^3}=\Pi_g\left(\frac{E_0}{E_s},\frac{\sigma_0}{\sigma_s},\frac{h_{max}}{\delta},\frac{E_L}{E_T},\frac{\sigma_{0L}}{\sigma_{0T}}\right) \quad \text{Eq 3-15}$$

where P_e and P_f are force on punch at different penetration displacement.

In this paper, $h_e/\delta=0.3$, $h_f/\delta=0.7$ and $h_{max}/\delta=1.0$ are chosen, i.e. $h_e=0.6\mu m$, $h_f=1.4\mu m$, $h_{max}=2.0\mu m$. Since h_r is also dependent on the same variables as W_u. Therefore equations (3-13) to (3-15) could be re-written as:

$$\frac{P_1}{\sigma_0 0.6\mu m^2}=\Pi_1\left(\frac{E_0}{E_s},\frac{\sigma_0}{\sigma_s},\frac{E_L}{E_T},\frac{\sigma_{0L}}{\sigma_{0T}}\right); \quad \text{Eq 3-16}$$

$$\frac{P_2}{\sigma_0 1.4\mu m^2}=\Pi_2\left(\frac{E_0}{E_s},\frac{\sigma_0}{\sigma_s},\frac{E_L}{E_T},\frac{\sigma_{0L}}{\sigma_{0T}}\right); \quad \text{Eq 3-17}$$

$$\frac{W_u}{\sigma_0 2\mu m^3} = \Pi_g\left(\frac{E_0}{E_s}, \frac{\sigma_0}{\sigma_s}, \frac{E_L}{E_T}, \frac{\sigma_{0L}}{\sigma_{0T}}\right); \qquad \text{Eq 3-18}$$

From now on, equations (3-16) to (3-18) or say, $P_1/(\sigma_0 * 0.6\mu m^2)$, $P_2/(\sigma_0 * 1.4\mu m^2)$ and $W_u/(\sigma_0 * 2\mu m^3)$ are identified as three characteristic parameters on the $\mathrm{P}-\mathrm{h}$ curve of instrumented indentation on transversely isotropic thin film.

3.2.2.2. Influence of plastic property σ_0

Before specific expressions for equations (3-16) to (3-18) are given, the intrinsic relationships among above three parameters and six variables are required for displaying. In Fig.3-6, how σ_0 (or how σ_0/σ_s) influence the results are demonstrated.

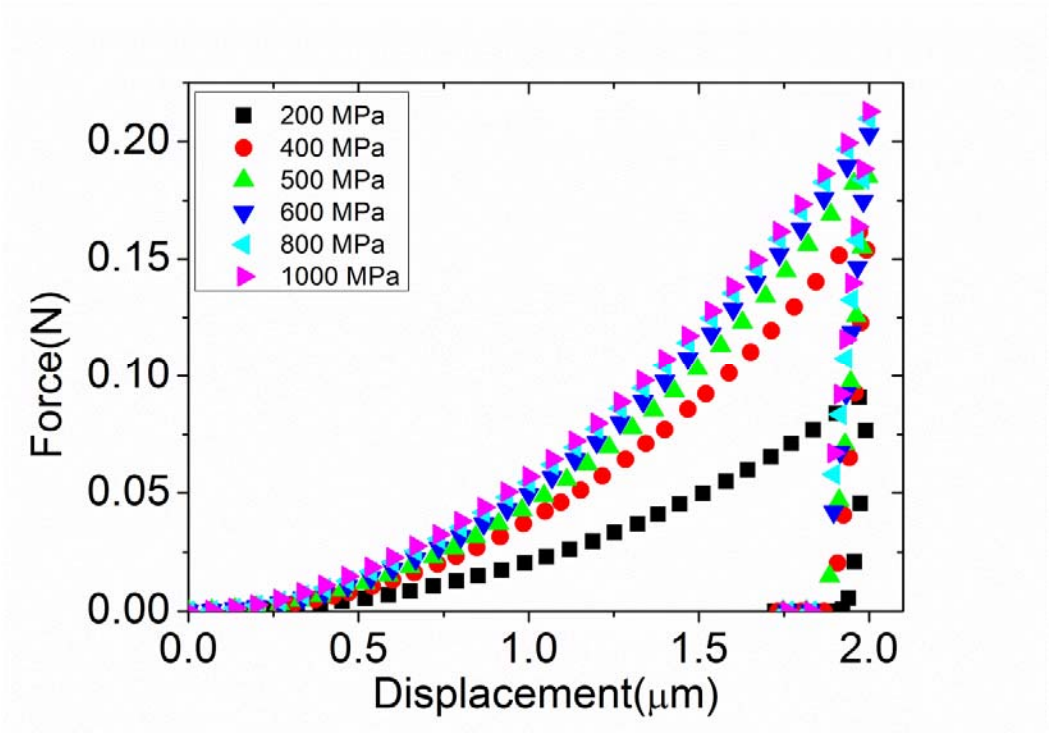

Figure 3-6: $\mathrm{P}-\mathrm{h}$ curve obtained from FEM results with film properties as $\mathrm{E_0} = 150\mathrm{GPa}$, $\mathrm{E_L/E_T} = 1.1$, $\sigma_{0\mathrm{L}}/\sigma_{0\mathrm{T}} = 1.2$ and σ_0 varies from 200MPa to 1000MPa.

Obviously, force P increases with σ_0, especially when σ_s is smaller than σ_0. But when σ_0 reaches a certain level, i.e. twice the value of σ_s here, the impact significantly weakened. This might be the basic reason why Chen and Zhao [29] claimed that when upper film is “soft”, results of forward and reverse analysis were more accurate. By applying section by section fitting method and fitting function of (3-7), more detailed

information about $\mathrm{P}-h$ curve is revealed, showing in (Fig.3-7). Regardless of the film material is “softer” or “harder”, respect to the substrate material, all the exponent increases with displacement h (when $h > 0.5\mu m$), this is because after strain hardening in substrate, yield stresses continuous to rise, therefore, even when σ_0 is initially greater than σ_s, i.e. when $\sigma_0 = 500MPa$ or $600MPa$, the exponent value turns to be larger than 2 after a period of time. Additionally, unlike in previous sections, even if penetrations displacement reaches 1.8 μm, the value of exponent still did not show any downward trend, for $\sigma_0 = 200MPa,\ 400MPa, 500MPa, 600MPa$. This might due to the mismatch between properties keeps growing, and the discordance amid stress distribution also become more intensive which cannot be eliminated with the increment of displacement.

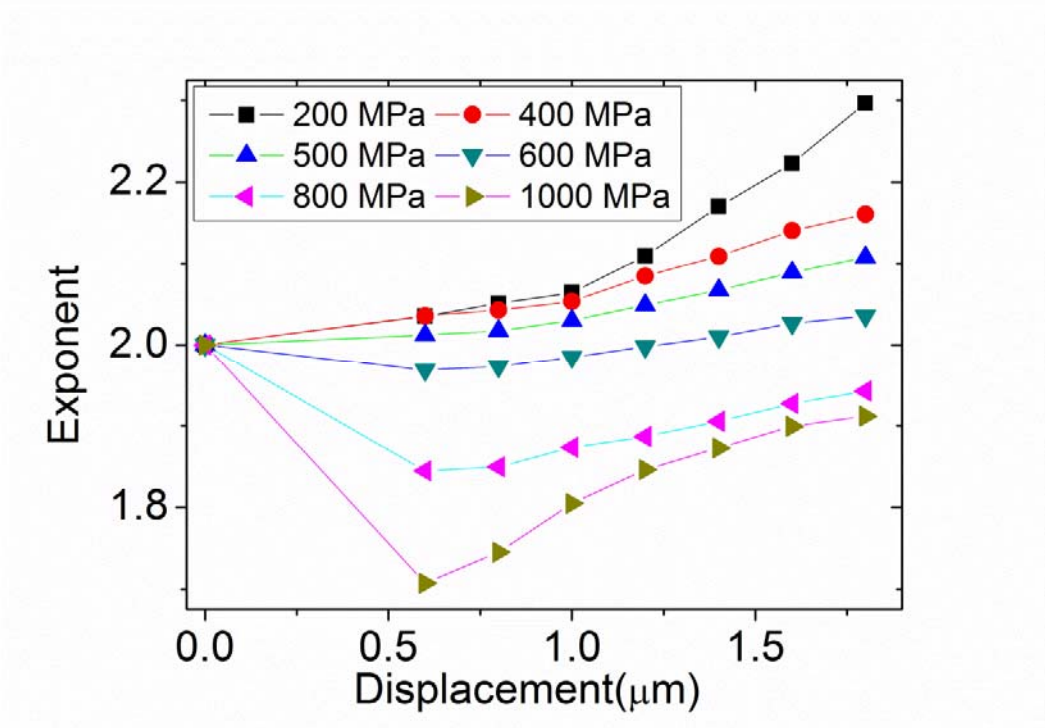

Figure 3-7: Fitting each curve in Fig.3-6 with equation (3-8) and applying section by section method. Exponent m at different displacement was obtained.

Substrate effect also played an important role in specimen hardness which can be seen from (Fig.3-8). While penetration displacement h was smaller than half the film thickness δ, then the specimen hardness was almost equal to topper film hardness.

Whereas h became greater than $\delta/2$, specimen hardness tended to approach the hardness value of substrate, although the change was slightly and slowly. Fig.3-9 demonstrated panorama of how hardness altered with σ_0. All values of hardness are closed to$3\sigma_0$, but slightly smaller.

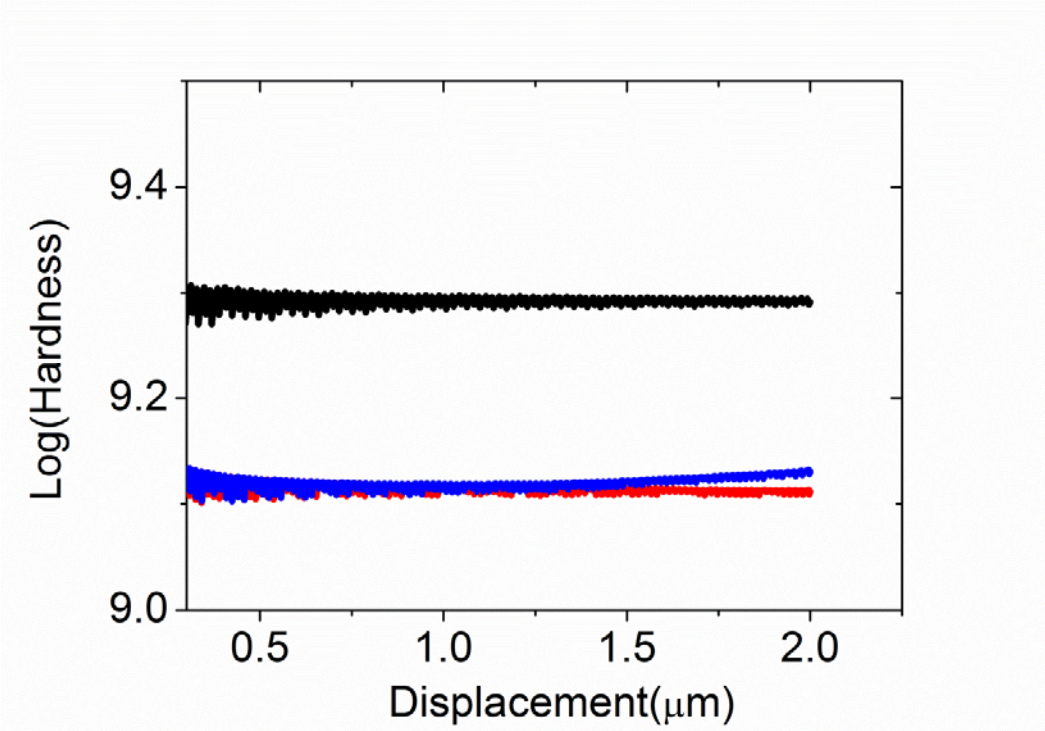

Figure 3-8: Schematic of hardness changes with increasing indenter displacement. Black line represents the result while cone indenter punch into a semi-infinite bulk specimens with its properties as same as the substrate. Red line is the result of the same type indenter punching into a semi-infinite bulk specimen with its properties as $E_0 = 150\mathrm{GPa}$, $\mathrm{E_L/E_T} = 1.1$, $\sigma_{0\mathrm{L}}/\sigma_{0\mathrm{T}} = 1.2$ and $\sigma_0 = 500\ MPa$. Blue line results from the indentation when the materials of red line work as upper film on the substrate.

σ_0 (or σ_0/σ_s) also affect three characteristic parameters (i.e. (3-16), (3-17), (3-18)) in different ways. Shown in Fig.3-10, again, certificated two points as above: first, smaller the value of σ_0, more sensitive the film are on substrate effect (from (Fig.3-10a) to (Fig.3-10c)); second, by comparing (Fig.3-10a) and (Fig.3-10b), obviously, at different displacement, the rules how σ_0 influence parameters were also different, which has verified once again that choosing the P values at diverse h as characteristic parameters was feasible.

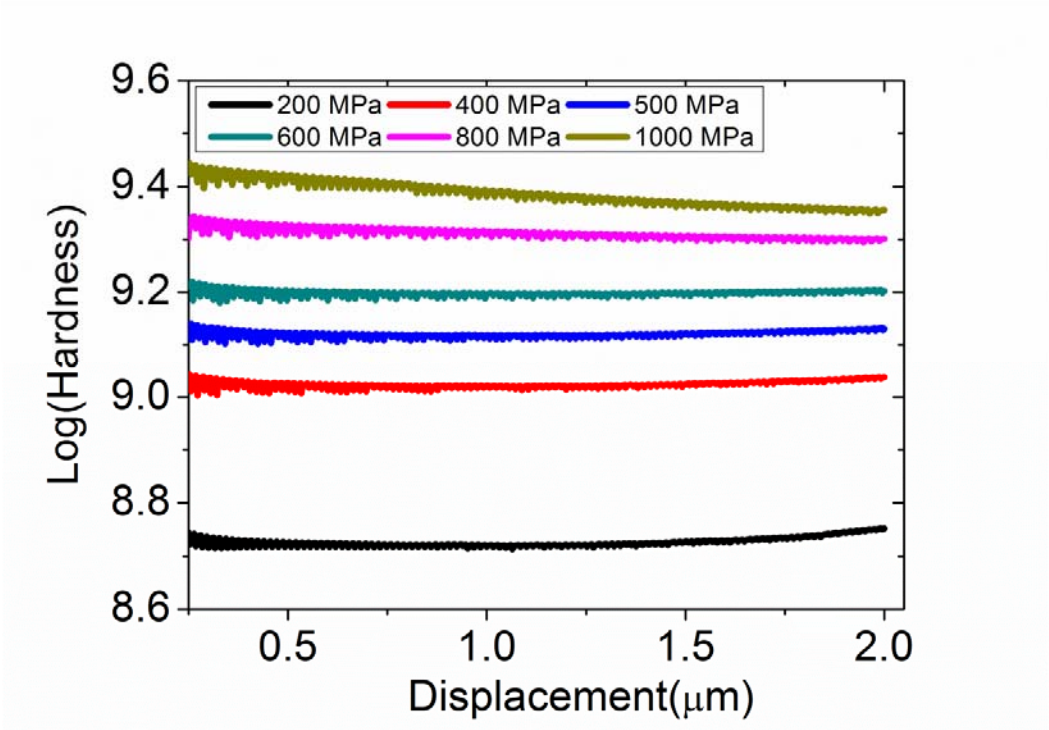

Figure 3-9: Schematic of hardness obtained from FEM result with film's properties as $E_0 = 150\text{GPa}$, $\text{E}_\text{L}/\text{E}_\text{T} = 1.1$, $\sigma_{0\text{L}}/\sigma_{0\text{T}} = 1.2$ and σ_0 varies from 200MPa to 1000MPa.

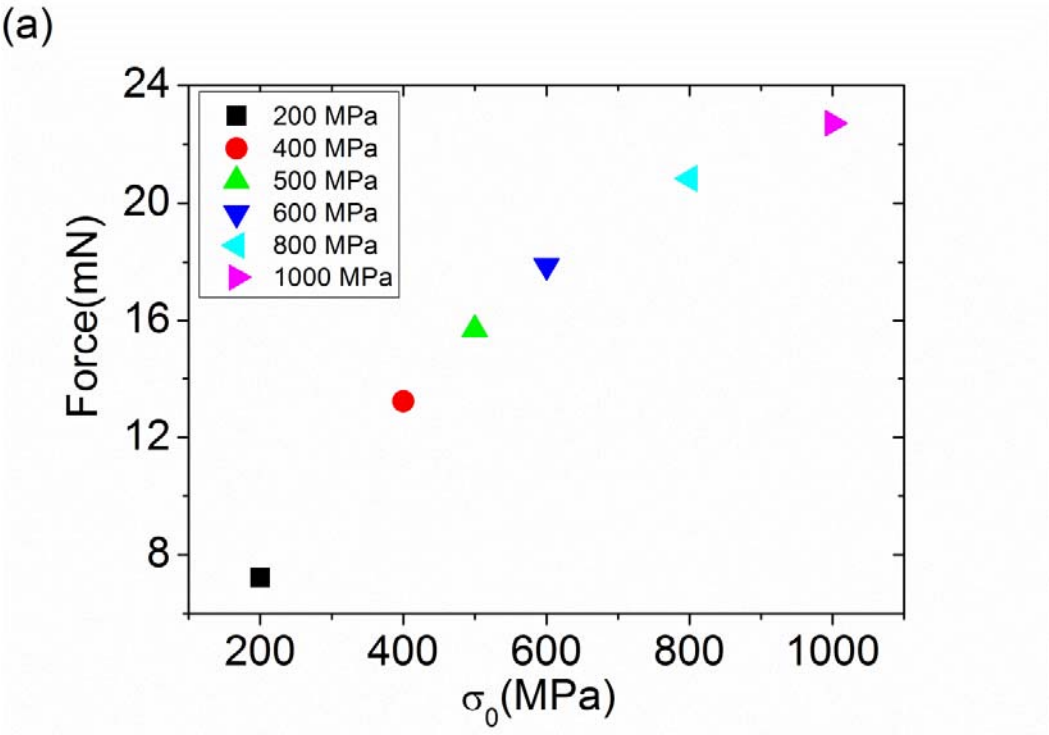

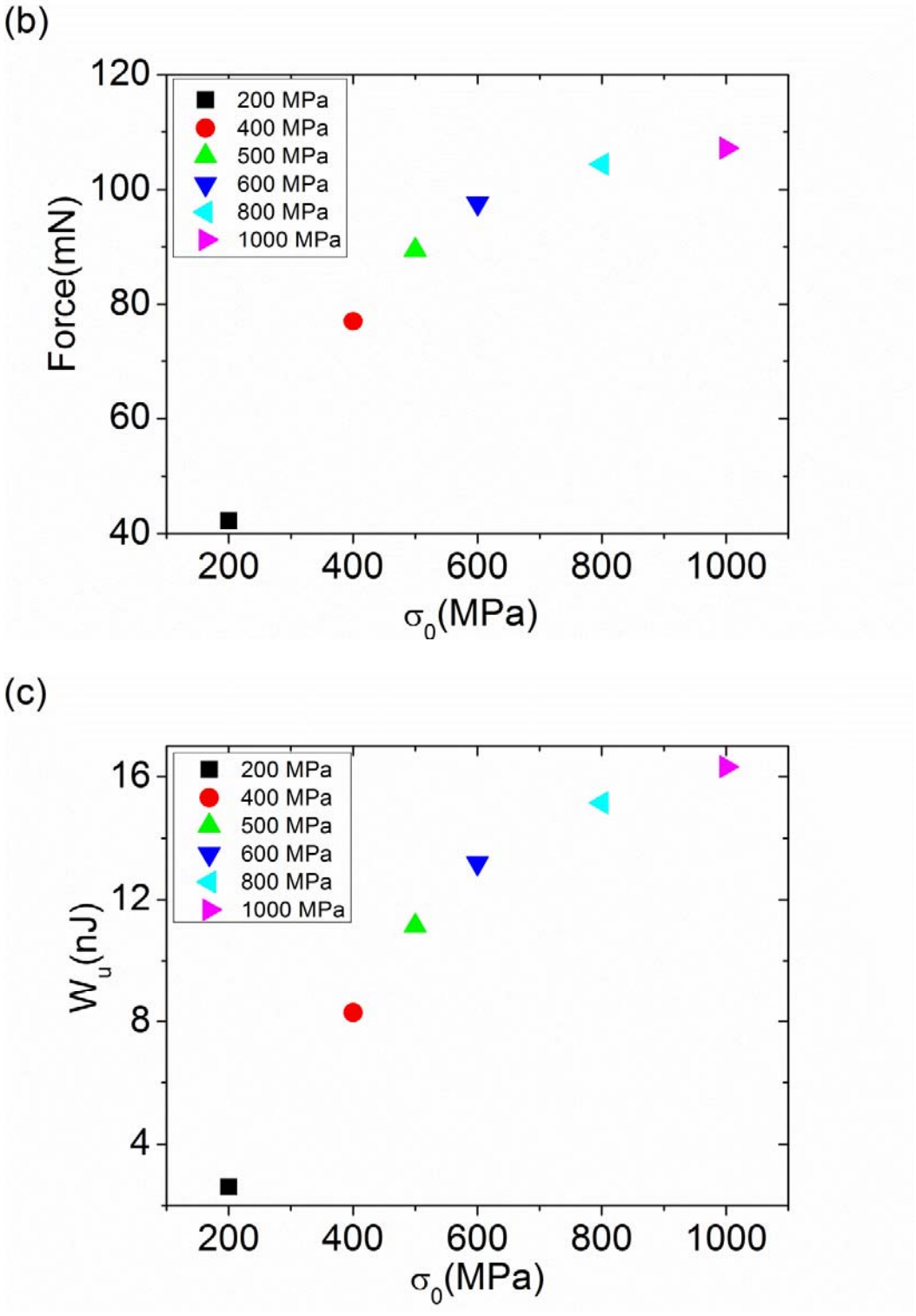

Figure 3-10: Varying value of σ_0 affected three characteristic parameters in different ways as properties of film were $E_0 = 150\text{GPa}$, $E_L/E_T = 1.1$, $\sigma_{0L}/\sigma_{0T} = 1.2$ and σ_0 varies from 200MPa to 1000MPa: (a) P_1 at $h = 0.6\mu\text{m}$, (b) P_2 at $h = 1.4\mu\text{m}$, (c) W_u at $h = 2\mu\text{m}$.

3.2.2.3. Influence of Young's modulus $\mathbf{E_0}$

From Fig.3-11, it can be seen that Young's modulus E_0 (or E_0/E_s) varying in films, indeed, affected $\mathrm{P}-h$ curve, although the influence is not as significant as yield stress, σ_0, does. From the partially enlarged figure, (i.e. Fig.3-12) the increment of Force P at same indenter displacement h, along with the increasing of film's Young's modulus, can be clearly observed. Exponent m obtained from each curve in Fig.3-11 was displayed in Fig.3-13. It's clear that after displacement greater than $0.6\mu\mathrm{m}$, all of them tend to grow, that is because the difference in σ_Y between film and substrate is slight, after the substrate start to deformation plastically, yield strength in it increases quickly, so the substrate became "harder", even when Young's modulus $\mathrm{E_0} = 250\ \mathrm{GPa}$ for the film.

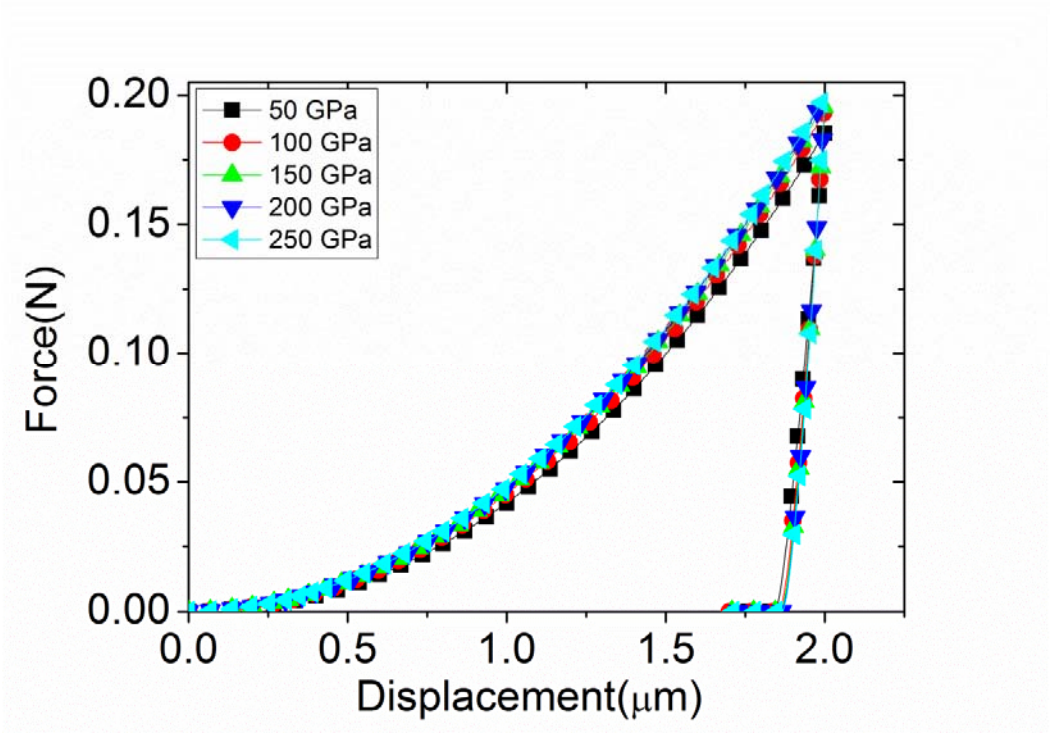

Figure 3-11: A picture of a series of $\mathrm{P}-\mathrm{h}$ curve obtained by FEM with film's properties set as $\sigma_0 = 500\mathrm{MPa}$,$E_L/E_T = 1.3$, $\sigma_{0L}/\sigma_{0T} = 1.4$ and E_0 varies from 50GPa to 200GPa.

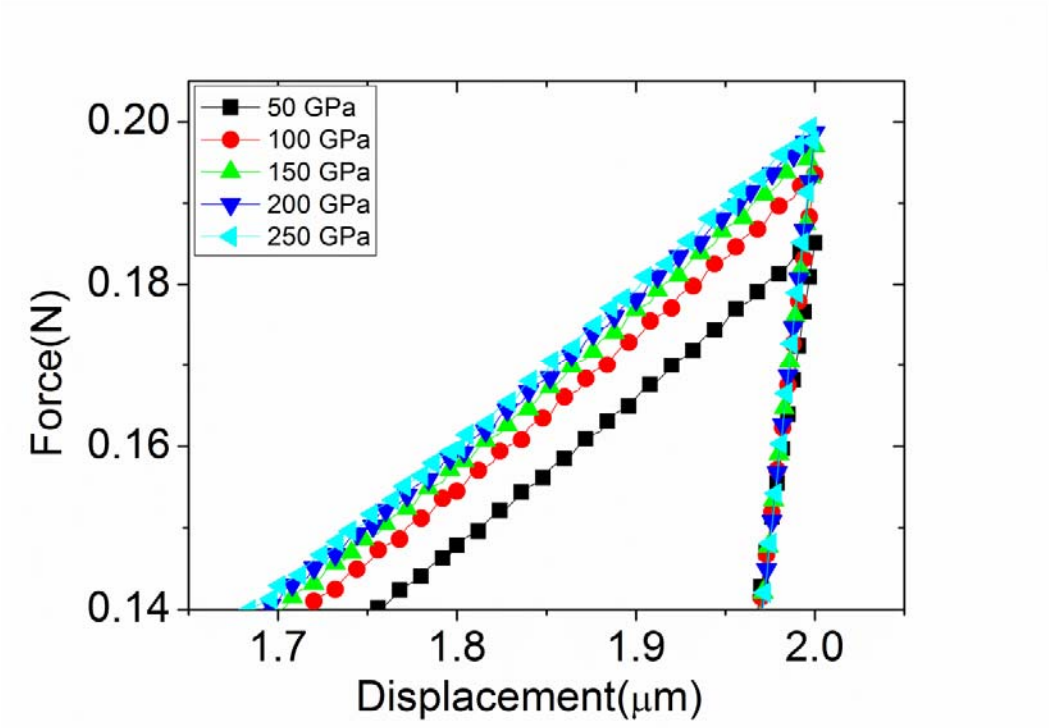

Figure 3-12: Partially enlarged figure of Fig.11 at the range from $\mathrm{h} = 1.7\mu\mathrm{m}$ to $\mathrm{h} = 2.0\mu\mathrm{m}$.

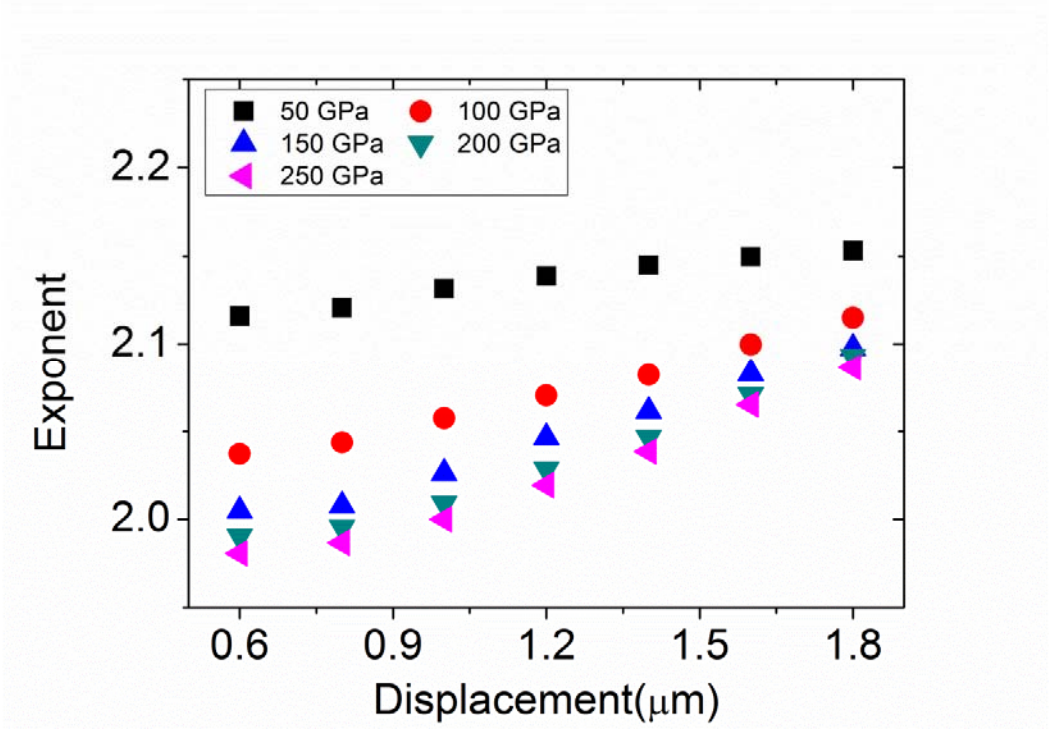

Figure 3-13: exponent m for each curve in Fig.3-11 when E_0 varies from 50GPa to 200GPa

Change trends of parameters equations (3-16) and (3-17) were show in Fig.3-14(a) and Fig3-14(b), both of them increase with E_0. Surprisingly, the value of parameter (3-18) actually decreases with the increase of film Young's modulus, which is shown in Fig.3-14(c). Change of film's Young's modulus has negligible influence on the hardness of the specimen even when displacement reaches 100% of film's thickness (illustrated in Fig.3-15).

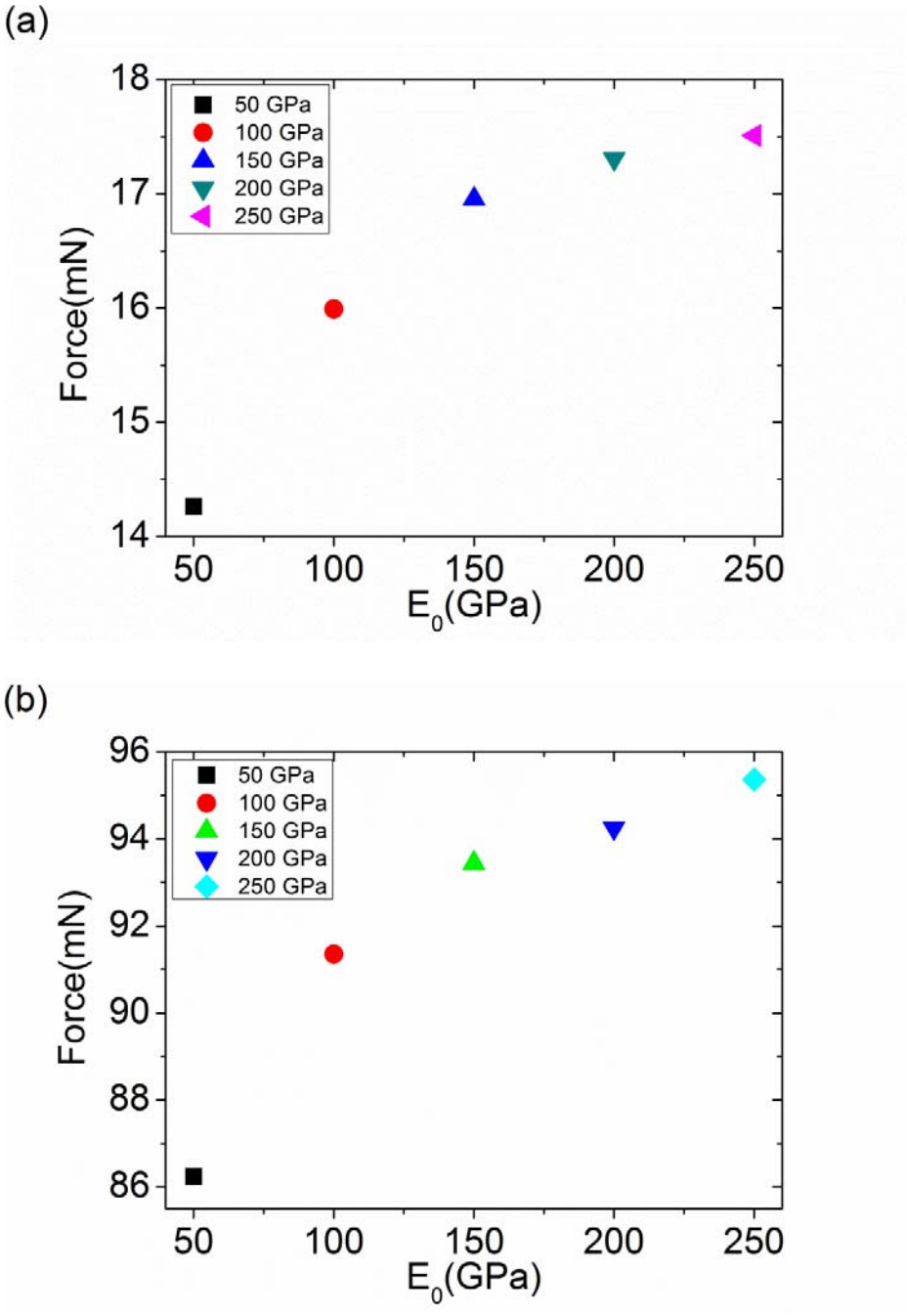

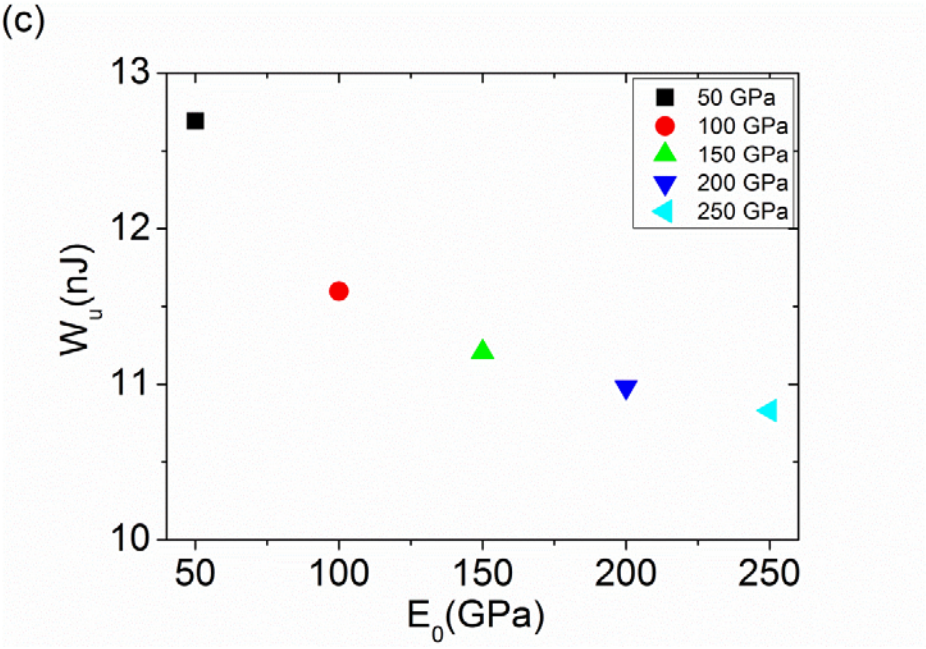

Figure 3-14: Varying value of E_0 affected three characteristic parameters in different ways as properties of film were $\sigma_0 = 500\text{MPa}$, $E_L/E_T = 1.3$, $\sigma_{0L}/\sigma_{0T} = 1.4$ and E_0 varies from 50GPa to 200GPa: (a) P_1 at $\text{h} = 0.6\mu\text{m}$, (b) P_2 at $\text{h} = 1.4\mu\text{m}$, (c) W_u at $\text{h} = 2\mu\text{m}$.

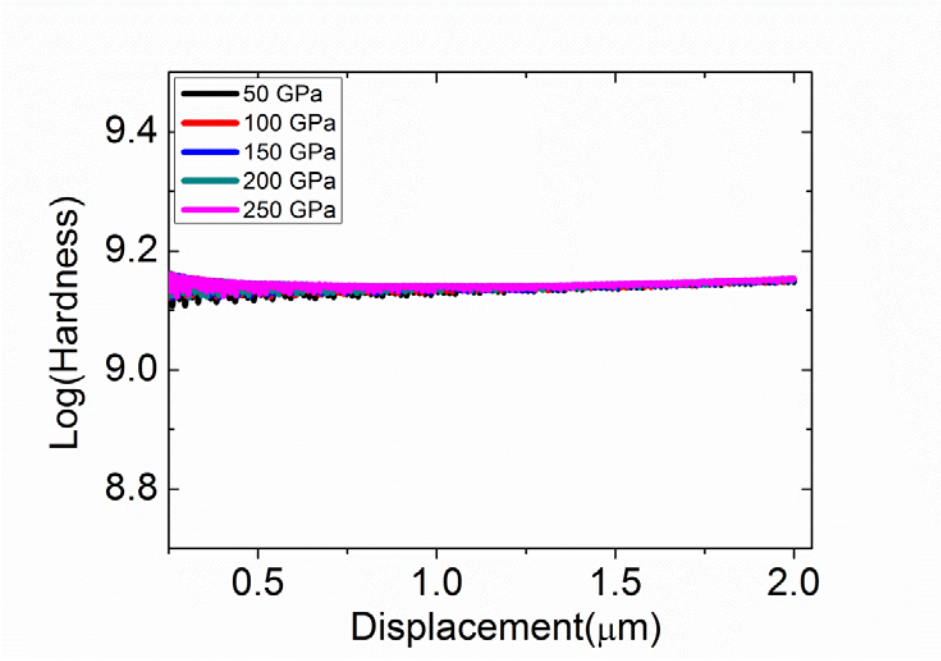

Figure 3-15: Hardness obtained by FEM with the properties of film set as $\sigma_0 = 500\text{MPa}$, $E_L/E_T = 1.3$, $\sigma_{0L}/\sigma_{0T} = 1.4$ and E_0 varies from 50GPa to 200GPa.

3.2.2.4. Influence of plastic anisotropy σ_{0L}/σ_{0T}

The plastic anisotropy σ_{0L}/σ_{0T} has a greater impact on the $\mathrm{P}-h$ curve, with respect to elastic anisotropy E_L/E_T (shown in Fig.3-16). With partially enlarged Fig.3-16 (i.e. Fig.3-17), it shows that, higher the value of σ_{0L}/σ_{0T}, larger the force P needed for penetration at the same displacement h. Besides, all three parameter (3-16), (3-17) and (3-18) rise with increase value of σ_{0L}/σ_{0T} (shown in Fig.3-18). Plastic anisotropy also makes specimen's hardness to shift from each other Fig.3-19. .

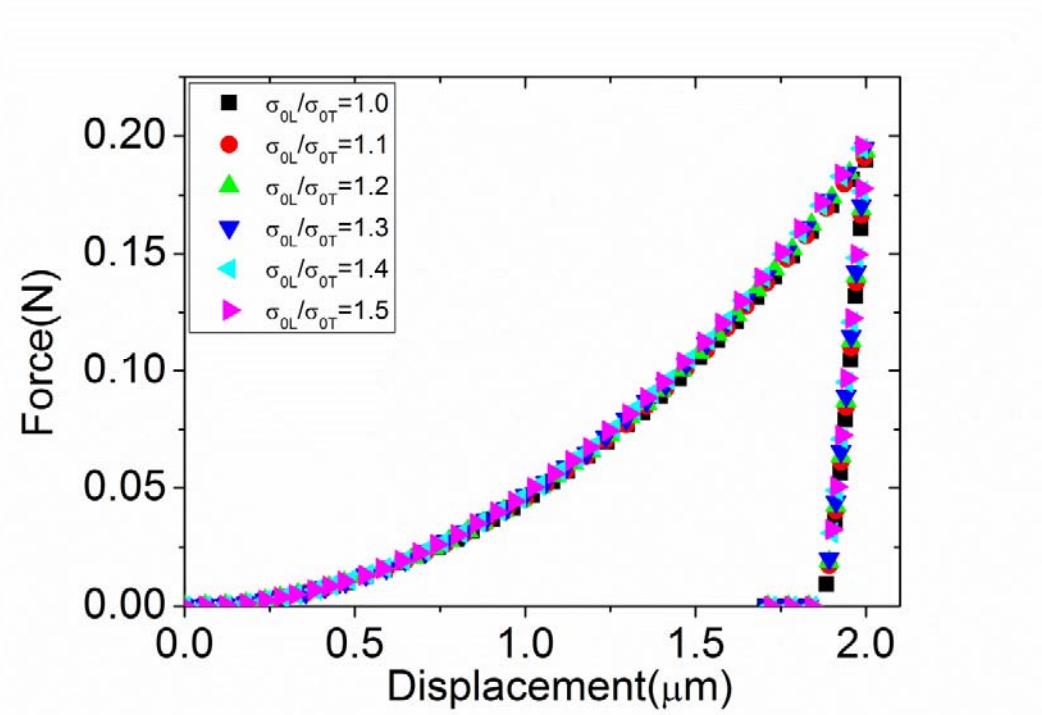

Figure 3-16: A series of $\mathrm{P}-\mathrm{h}$ curve obtained by FEM with film properties set as $\mathrm{E_0}=150\mathrm{GPa}$, $\sigma_0=500\mathrm{MPa}$, $E_L/E_T=1.0$, σ_{0L}/σ_{0T} varies from 1.0 to 1.5.

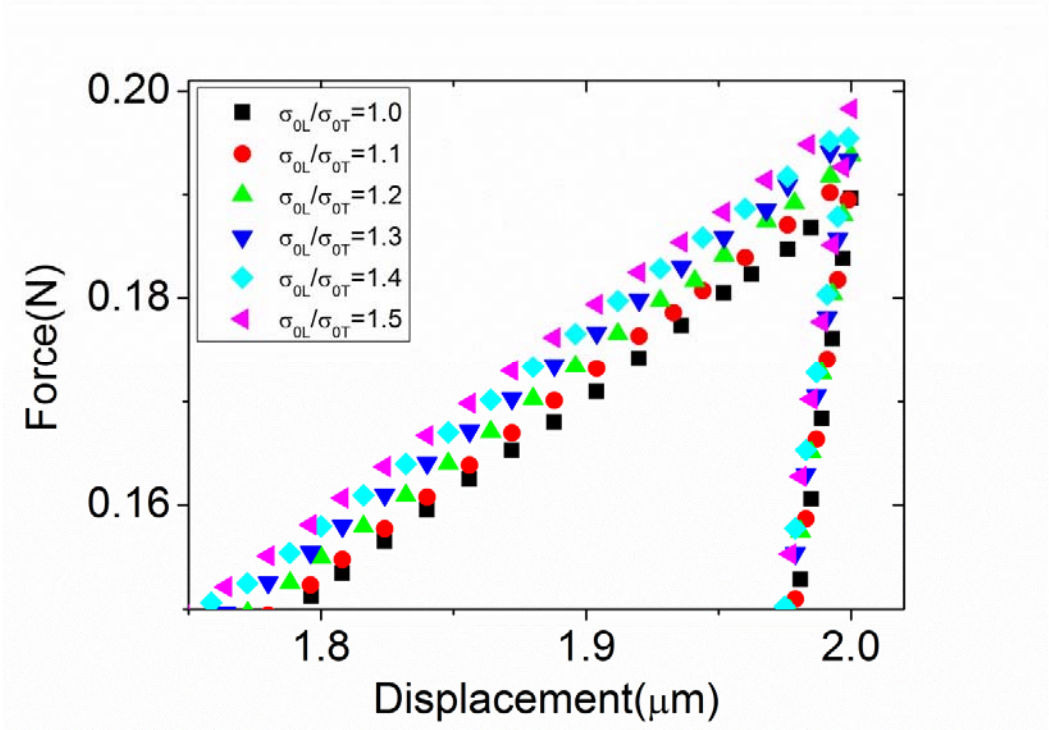

Figure 3-17: Partially enlarged figure of Fig.16 at the range from $\mathrm{h} = 1.75\mu\mathrm{m}$ to $\mathrm{h} = 2.0\mu\mathrm{m}$

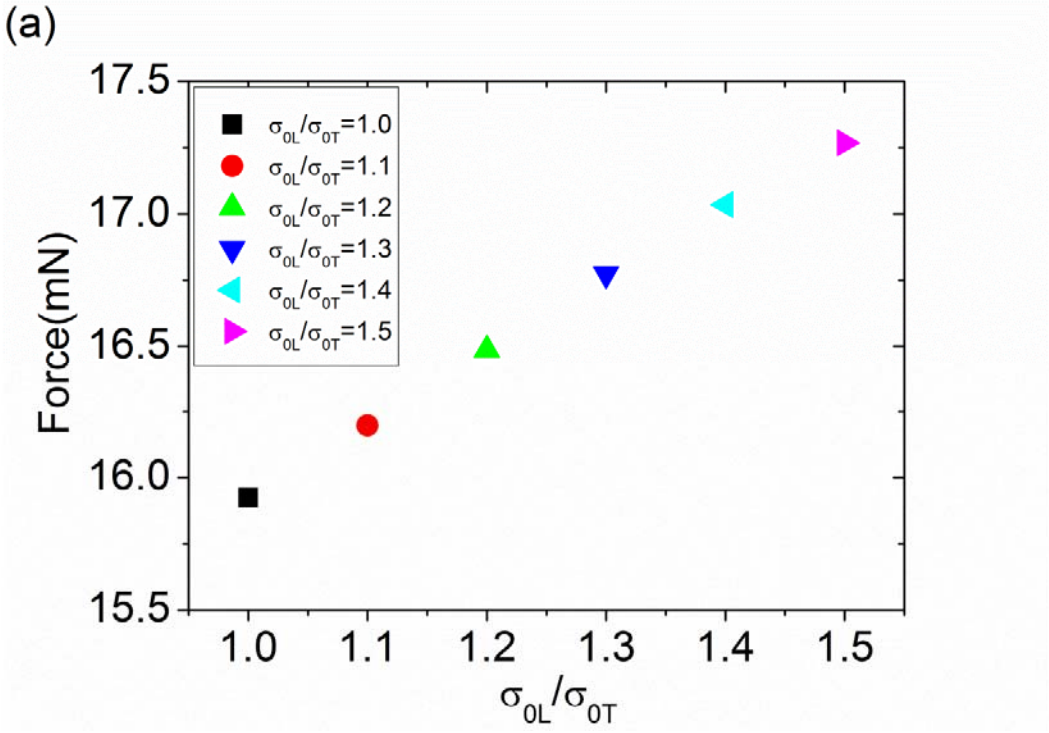

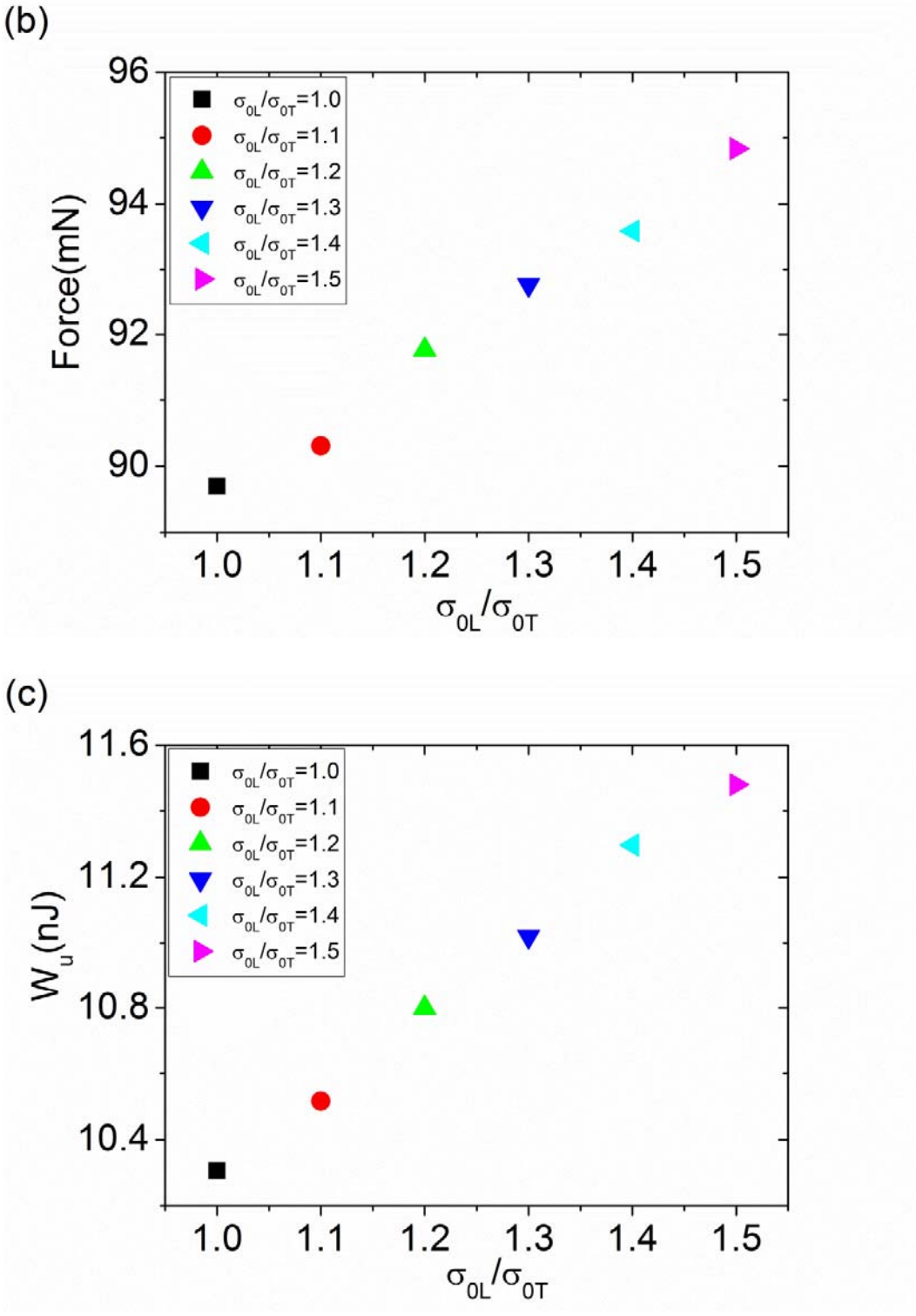

Figure 3-18: Growth of σ_{0L}/σ_{0T} makes all three characteristic parameters increase, when other properties fixed as $\mathrm{E_0} = 150\mathrm{GPa},\ \sigma_0 = 500\mathrm{MPa}, E_L/E_T = 1.0$ (a) $\mathrm{P_1}$ at $\mathrm{h} = 0.6\mu\mathrm{m}$, (b) $\mathrm{P_2}$ at $\mathrm{h} = 1.4\mu\mathrm{m}$, (c) $\mathrm{W_u}$ at $\mathrm{h} = 2\mu\mathrm{m}$.

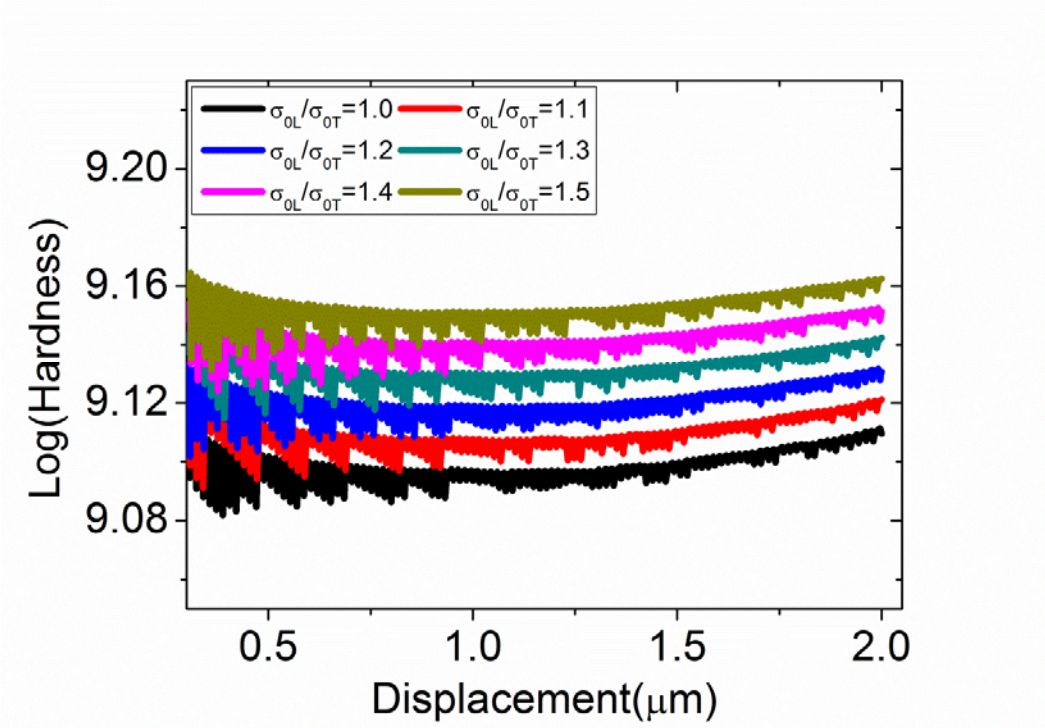

Figure 3-19: Hardness obtained by FEM with the properties of film set as $\mathrm{E}_0 = 150\mathrm{GPa}$, $\sigma_0 = 500\mathrm{MPa}$, $E_L/E_T = 1.0$, σ_{0L}/σ_{0T} varies from 1.0 to 1.5.

3.2.2.5. Influence of plastic anisotropy $\mathbf{E_L/E_T}$

The impact of elastic anisotropy E_L/E_T on the $\mathrm{P}-\mathrm{h}$ curve cannot be distinguished on an integral load-unload graph (Fig.3-20). Even in the partially enlarged figure, the difference between each curve is tiny (Fig.3-21). However, interesting, the elastic anisotropy E_L/E_T has an opposite impact on $\mathrm{P}-\mathrm{h}$ curve, with respect to σ_{0L}/σ_{0T}. More detailed influence on the three characteristic parameters i.e. equation (3-16) to (3-18) can be read from Fig.3-22. As same as the E_0, the effect of E_L/E_T on the hardness of specimen could almost be ignored as in Fig.3-23.

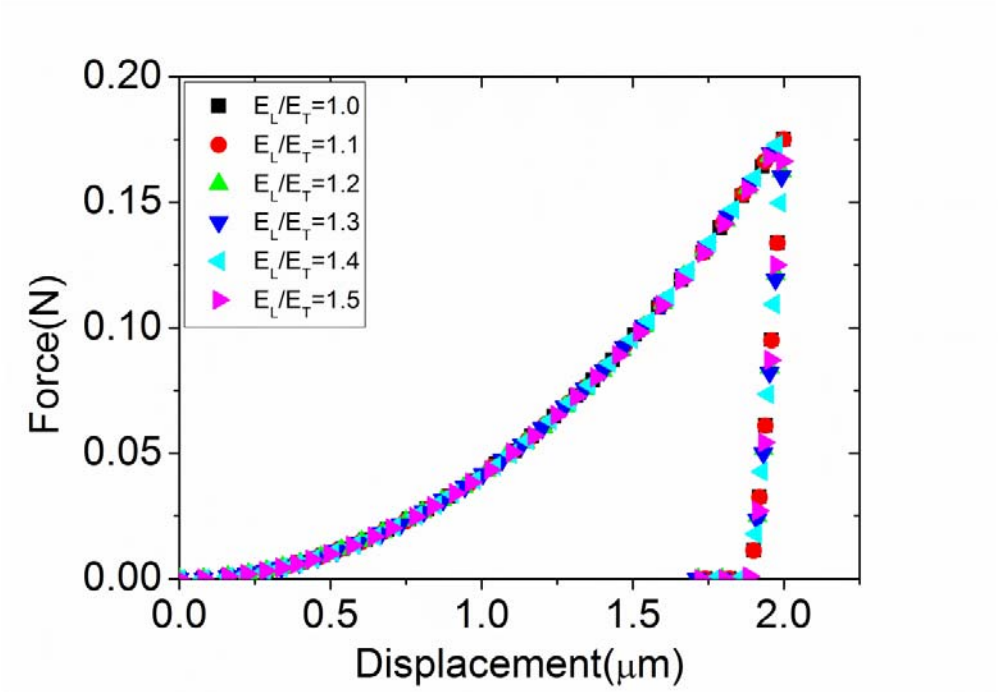

Figure 3-20: A series of $\mathrm{P}-h$ curve obtained by FEM with film's properties set as $E_0 = 200GPa$, $\sigma_0 = 400\mathrm{MPa}$, $\sigma_{0L}/\sigma_{0T} = 1.5$, E_L/E_T varies from 1.0 to 1.5.

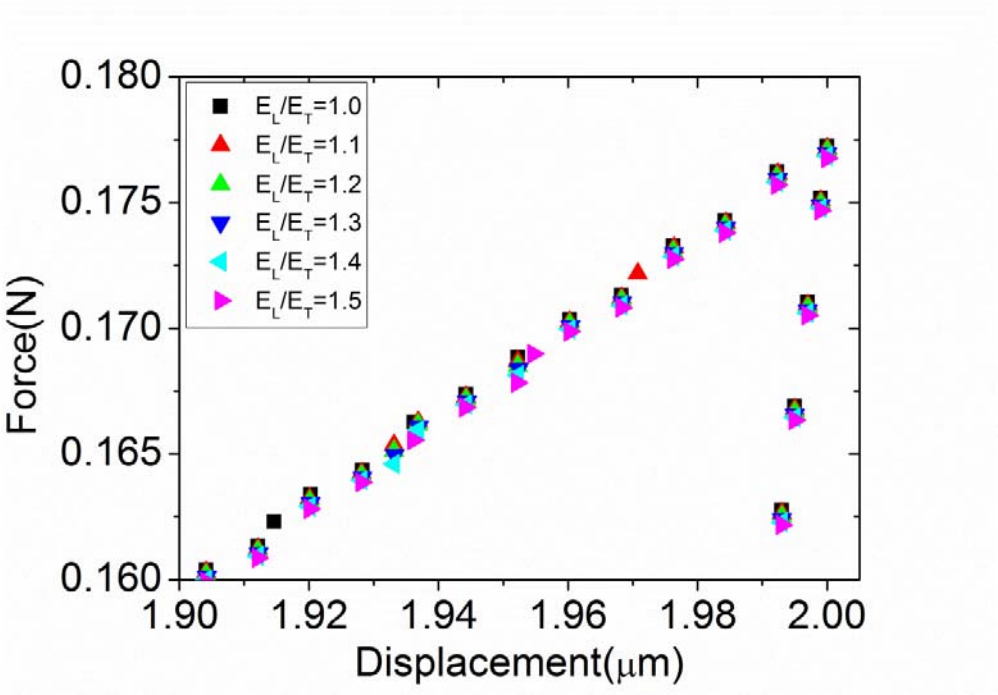

Figure 3-21: Partially enlarged figure of Fig.20 at the range of $h = 1.9\mu m$ to $h = 2.0\mu m$.

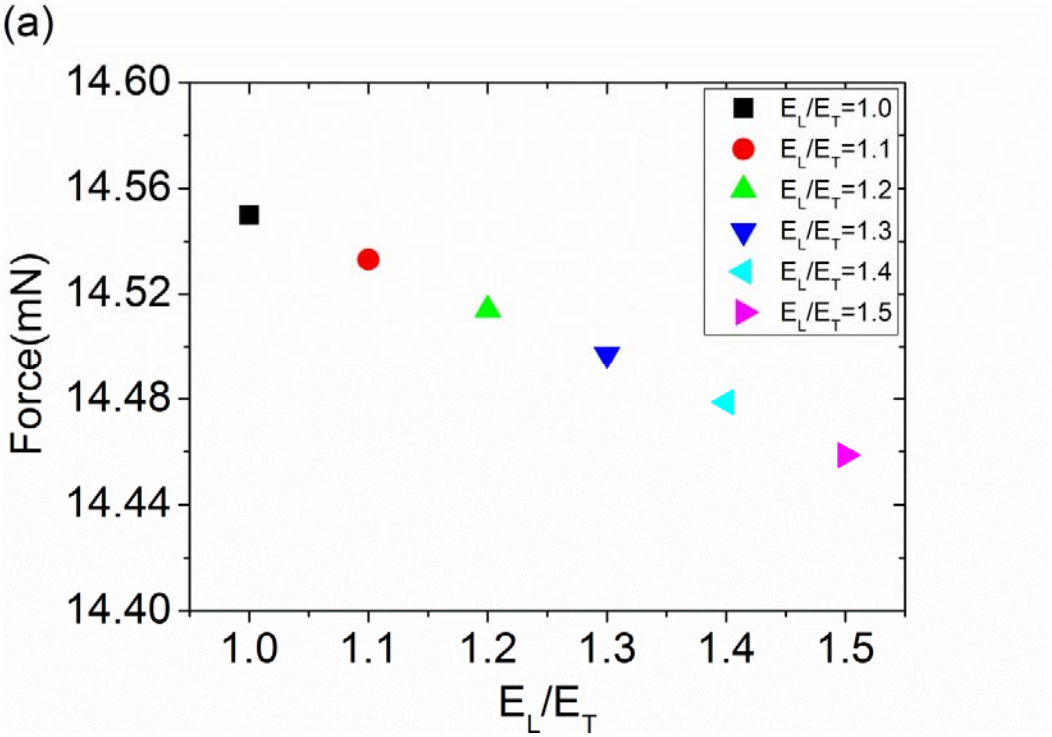
(a)
14.60
14.56
14.52
14.48
14.44
14.40
Force(mN)
1.0
1.1
1.2
1.3
1.4
1.5
E_L/E_T
E_L/E_T=1.0
E_L/E_T=1.1
E_L/E_T=1.2
E_L/E_T=1.3
E_L/E_T=1.4
E_L/E_T=1.5

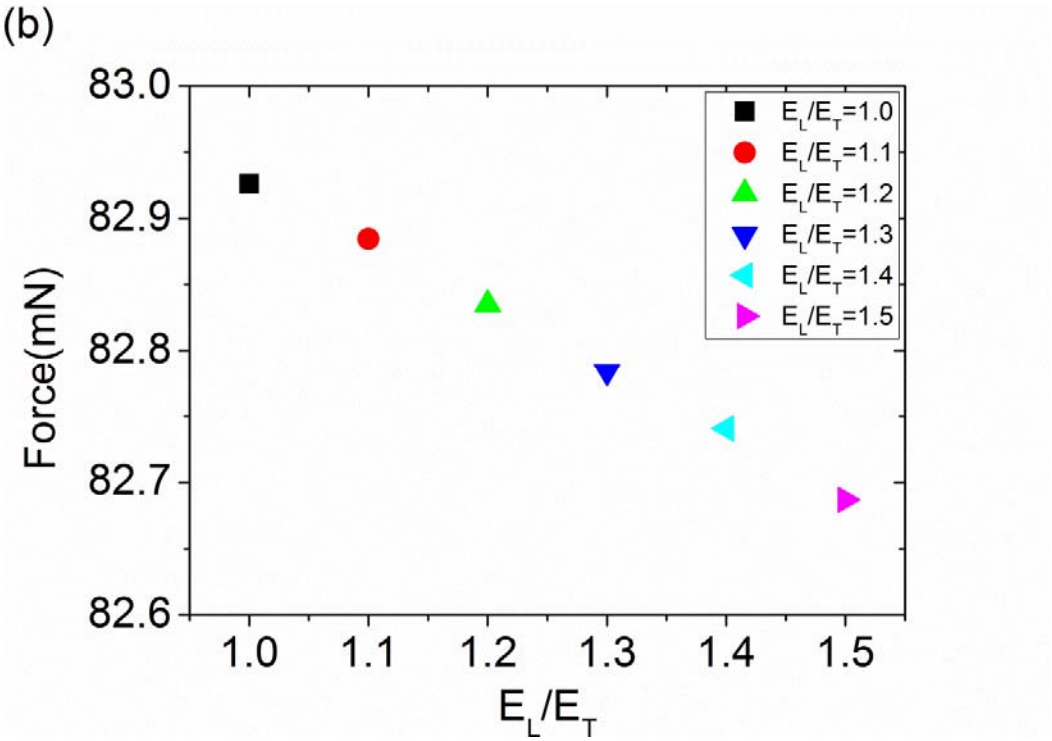
(b)
83.0
82.9
82.8
82.7
82.6
Force(mN)
1.0
1.1
1.2
1.3
1.4
1.5
E_L/E_T
E_L/E_T=1.0
E_L/E_T=1.1
E_L/E_T=1.2
E_L/E_T=1.3
E_L/E_T=1.4
E_L/E_T=1.5

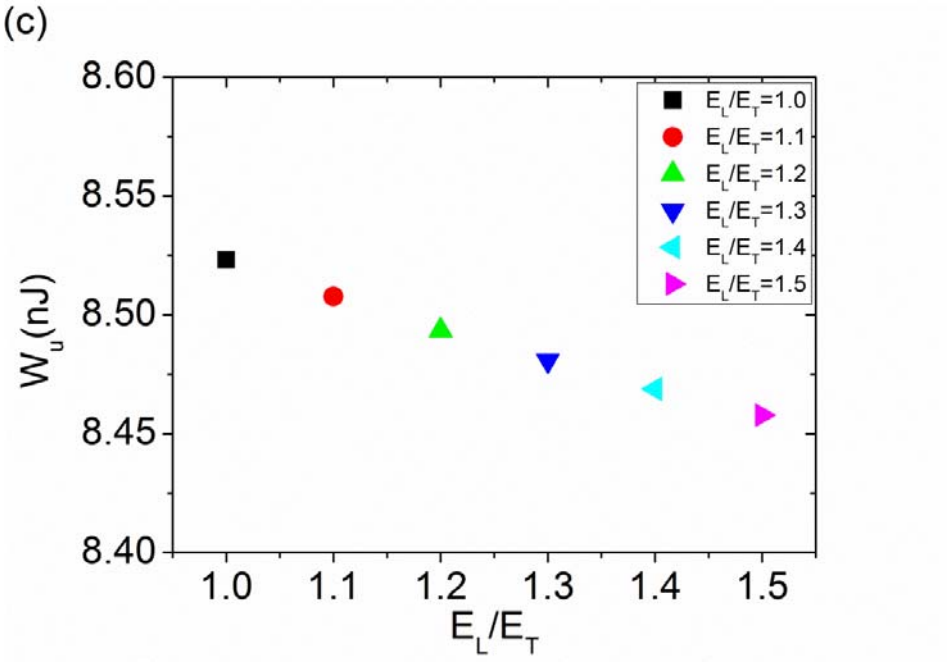

Figure 3-22: Growth of E_L/E_T makes all three characteristic parameters decrease, while other variables fixed as $E_0 = 200GPa,\ \sigma_0 = 400\text{MPa}, \sigma_{0L}/\sigma_{0T} = 1.5$, (a) P_1 at $h = 0.6\mu\text{m}$, (b) P_2 at $h = 1.4\mu\text{m}$, (c) W_u at $h = 2\mu\text{m}$.

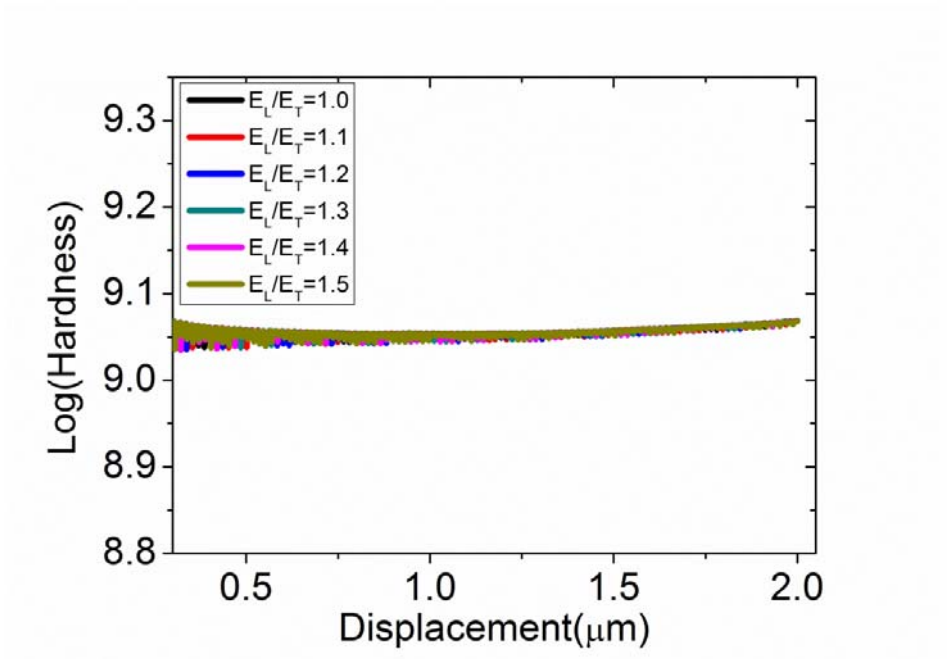

Figure 3-23: Hardness obtained by FEM with the properties of film set at $E_0 = 200GPa,\ \sigma_0 = 400\text{MPa}, \sigma_{0L}/\sigma_{0T} = 1.5$, and E_L/E_T varies from 1.0 to 1.5.

3.2.2.6. Combined effects of σ_{0L}/σ_{0T} and E_L/E_T, or σ_0 and E_0

In order to research connections between four variables and to see how plastic anisotropy σ_{0L}/σ_{0T}, together with elastic anisotropy E_L/E_T , affects parameters (3-14) to (3-16), or how plastic property σ_{Y0} and elastic property E_0 works along with each other, 3D graphs are required. (Fig.3-24) and (Fig.3-25) shows the interaction between σ_{0L}/σ_{0T} and E_L/E_T, σ_0 and E_0, respectively.

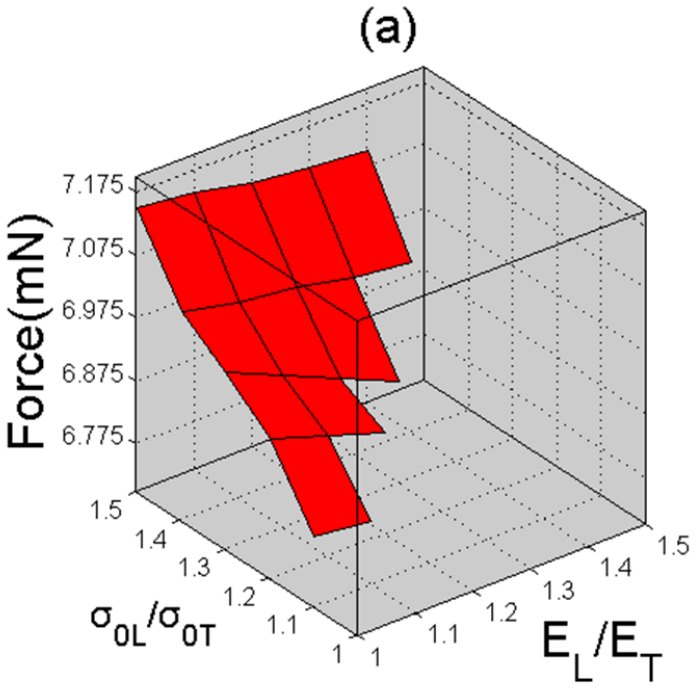

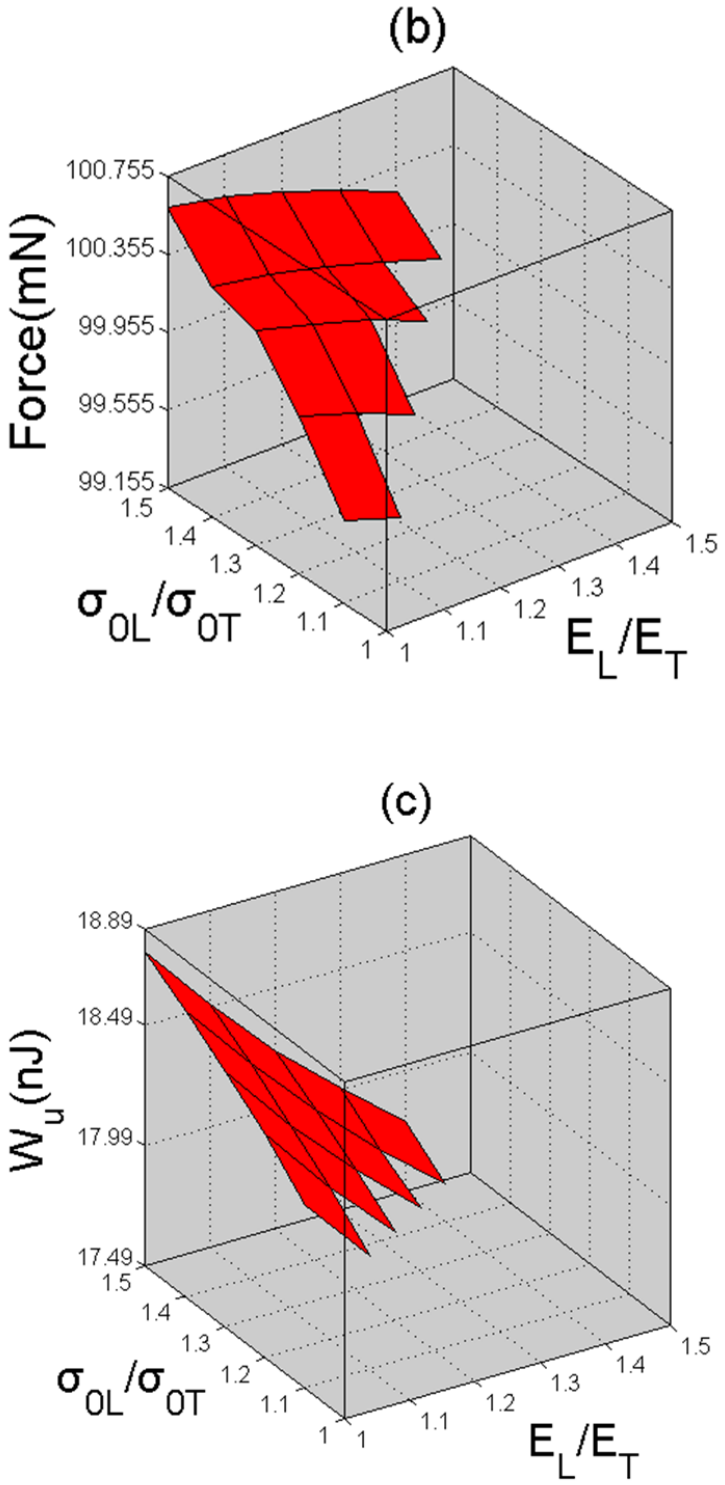

Figure 3-24: FEM results of three parameters with $\sigma_0 = 1000\text{MPa}$, $\text{E}_0 = 50\text{GPa}$ at varying value of $\text{E}_\text{L}/\text{E}_\text{T}$ and $\sigma_{0\text{L}}/\sigma_{0\text{T}}$

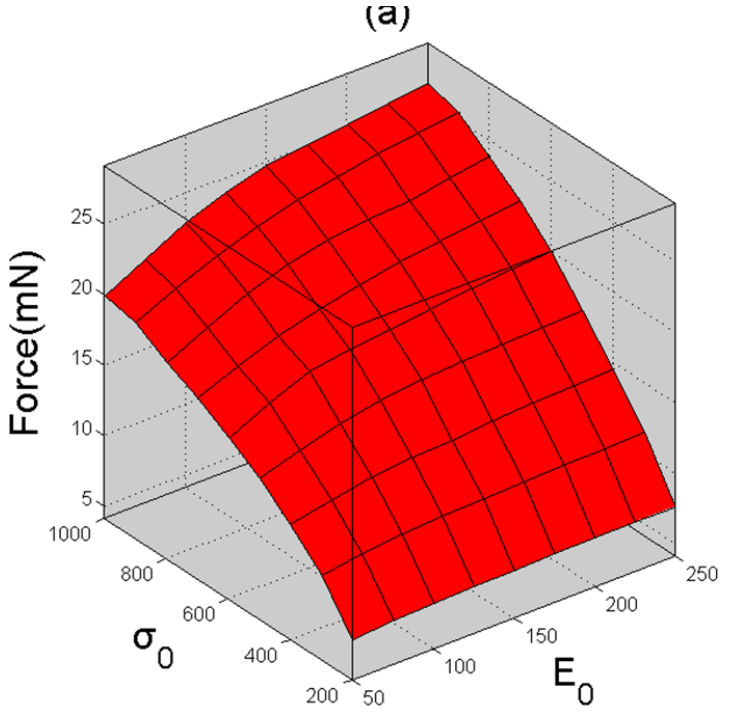
(a)
Force(mN)
25
20
15
10
5
1000
800
600
400
200
σ0
50
100
150
200
250
E0

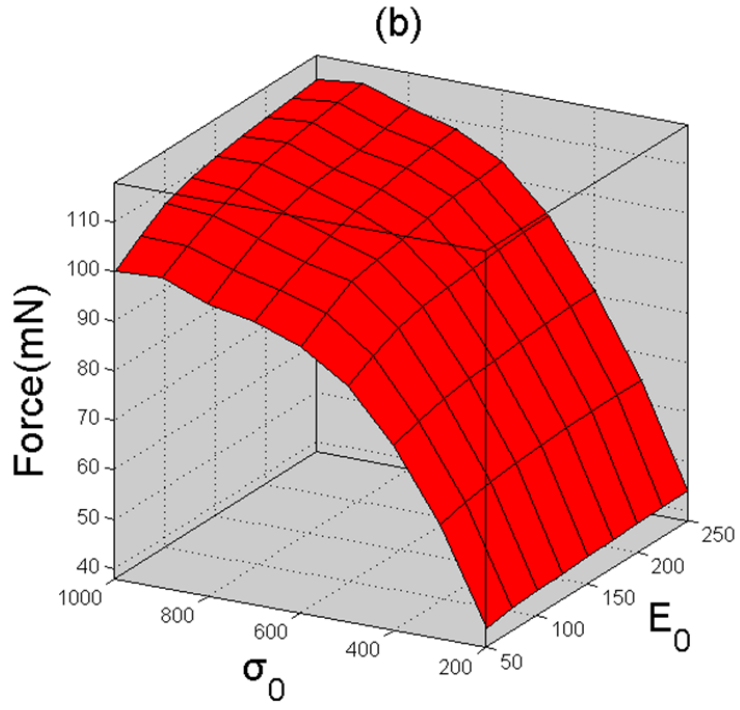
(b)
Force(mN)
110
100
90
80
70
60
50
40
1000
800
600
400
200
σ0
50
100
150
200
250
E0

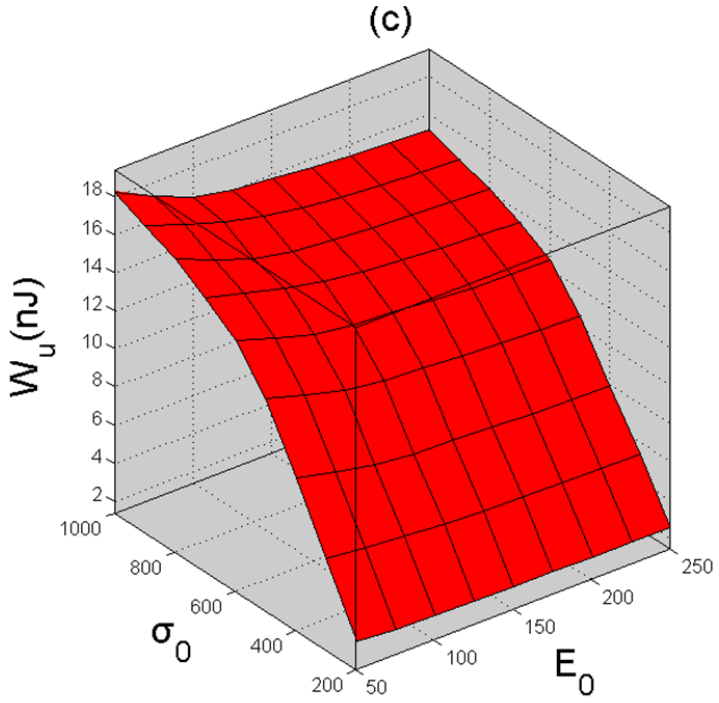

Figure 3-25: FEM results of three parameters with $\mathrm{E_L}/\mathrm{E_T} = 1.1$, $\sigma_{0\mathrm{L}}/\sigma_{0\mathrm{T}} = 1.3$, at different values of E_0 and σ_0

Two important conclusions could be gotten here. First, variables affect three parameters in different ways. Second, most effects are nonlinear.

3.2.3. Forward analysis

3.2.3.1. Forward analysis equation

By fitting all 630 sets of dates, equations Π_1, Π_2 and Π_3 are given in the forms as:

$$\Pi_1 = a_1^1 + a_1^2 x + a_1^3 y + a_1^4 z + a_1^5 w + a_1^6 x^2 + a_1^7 xy + a_1^8 xz + a_1^9 xw + a_1^{10} y^2 + a_1^{11} yz + a_1^{12} yw + a_1^{13} z^2 + a_1^{14} zw + a_1^{15} w^2 + a_1^{16} x/y + a_1^{17} x^2/y^2 + a_1^{18} y/x + a_1^{19} y^2/x^2 + a_1^{20} x^3 + a_1^{21} y^3 + a_1^{22} z^3 + a_1^{23} w^3 + a_1^{24} y/w + a_1^{25} y^2/w^2 + a_1^{26} x/z + a_1^{27} x^2/z^2; \quad \text{Eq 3-19}$$

$$\Pi_2 = a_2^1 + a_2^2 x + a_2^3 y + a_2^4 z + a_2^5 w + a_2^6 x^2 + a_2^7 xy + a_2^8 xz + a_2^9 xw + a_2^{10} y^2 + a_2^{11} yz + a_2^{12} yw + a_2^{13} z^2 + a_2^{14} zw + a_2^{15} w^2 + a_2^{16} x/y + a_2^{17} x^2/y^2 + a_2^{18} y/x + a_2^{19} y^2/x^2 + a_2^{20} x^3 + a_2^{21} y^3 + a_2^{22} z^3 + a_2^{23} w^3 + a_2^{24} y/w + a_2^{25} y^2/w^2 + a_2^{26} x/z + a_2^{27} x^2/z^2; \quad \text{Eq 3-20}$$

$$\Pi_3 = a_3^1 + a_3^2 x + a_3^3 y + a_3^4 z + a_3^5 w + a_3^6 x^2 + a_3^7 xy + a_3^8 xz + a_3^9 xw + a_3^{10} y^2 + a_3^{11} yz + a_3^{12} yw + a_3^{13} z^2 + a_3^{14} zw + a_3^{15} w^2 + a_3^{16} x/y + a_3^{17} x^2/y^2 + a_3^{18} y/x + a_3^{19} y^2/x^2 + a_3^{20} x^3 + a_3^{21} y^3 + a_3^{22} z^3 + a_3^{23} w^3 + a_3^{24} y/w + a_3^{25} y^2/w^2 + a_3^{26} x/z + a_3^{27} x^2/z^2 + a_3^{28} z/x + a_3^{29} z^2/x^2 + a_3^{30} w/y + a_3^{31} w^2/y^2 + a_3^{32} y/z + a_3^{33} y^2/z^2 + a_3^{34} x/w + a_3^{35} x^2/w^2; \quad \text{Eq 3-21}$$

Here the numbers in the subscript represent three different characteristic parameters, and the numbers in the superscript represent the item numbers in equations. Additionally, $\mathrm{x}, \mathrm{y}, \mathrm{z}, \mathrm{w}$, respectively, represent the properties parameters $\frac{\mathrm{E_0}}{\mathrm{E_S}}$, $\frac{\sigma_0}{\sigma_S}$, $\frac{\mathrm{E_L}}{\mathrm{E_T}}$, $\frac{\sigma_{0\mathrm{L}}}{\sigma_{0\mathrm{T}}}$. The complete sets of coefficients before each item are provided in (Table 3-2).

Table 3-2: Coefficient in functions of three characteristic parameters

Coefficient of function Π_1				Coefficient of function Π_2				Coefficient of function Π_3			
a_1^1	83.7614	a_1^{19}	0.9884	a_2^1	46.9682	a_2^{19}	0.628	a_3^1	-2.6445	a_3^{19}	0.0026
a_1^2	20.0178	a_1^{20}	0.9728	a_2^2	57.042	a_2^{20}	0.039	a_3^2	-7.9735	a_3^{20}	0.0378
a_1^3	6.1124	a_1^{21}	1.9112	a_2^3	-4.7022	a_2^{21}	11.5492	a_3^3	4.7507	a_3^{21}	1.5927
a_1^4	-11.4396	a_1^{22}	-0.8759	a_2^4	1.4757	a_2^{22}	0.9512	a_3^4	-2.3881	a_3^{22}	-0.1626
a_1^5	-0.6373	a_1^{23}	-2.3229	a_2^5	-0.299	a_2^{23}	-2.0572	a_3^5	-0.0495	a_3^{23}	-0.9371
a_1^6	5.3153	a_1^{24}	15.6592	a_2^6	-3.2112	a_2^{24}	46.655	a_3^6	0.9637	a_3^{24}	-0.6514
a_1^7	-2.0772	a_1^{25}	-3.2224	a_2^7	2.9597	a_2^{25}	-7.4217	a_3^7	16.2591	a_3^{25}	-0.1524
a_1^8	-6.9102	a_1^{26}	-5.8802	a_2^8	-3.638	a_2^{26}	-2.4303	a_3^8	-0.8339	a_3^{26}	-1.1929
a_1^9	-0.2654	a_1^{27}	0.7429	a_2^9	0.1499	a_2^{27}	0.5212	a_3^9	0.109	a_3^{27}	0.1399
a_1^{10}	-6.8623			a_2^{10}	-43.9762			a_3^{10}	-8.5033	a_3^{28}	0.5147
a_1^{11}	12.9493			a_2^{11}	1.0809			a_3^{11}	0.8006	a_3^{29}	-0.0487
a_1^{12}	1.7569			a_2^{12}	0.961			a_3^{12}	0.0332	a_3^{30}	2.2801
a_1^{13}	-1.7531			a_2^{13}	0.2005			a_3^{13}	-0.1005	a_3^{31}	-0.3008
a_1^{14}	-2.5321			a_2^{14}	-2.1302			a_3^{14}	0.1627	a_3^{32}	0.6448
a_1^{15}	-4.1832			a_2^{15}	0.0593			a_3^{15}	-0.2832	a_3^{33}	-0.0825
a_1^{16}	-0.5988			a_2^{16}	-0.1658			a_3^{16}	0.4031	a_3^{34}	0.34
a_1^{17}	-0.0884			a_2^{17}	-0.0233			a_3^{17}	-0.0246	a_3^{35}	-0.0504
a_1^{18}	-11.0448			a_1^{18}	-6.7801			a_3^{18}	-0.0547		

3.2.3.2. Forward analysis results

To confirm the accuracy and practicability of the equations above, 16 new sets of materials properties were tested. By comparing the values of characteristic parameters getting from forward analysis equations to the results of FEM, as listed in (Table 3-2), good match was found. Here, the error is defined as $\left|\left(V_{forword}-V_{FEM}\right)/V_{FEM}\right|$. It's obviously these prediction results are reliable and have a very high precision, if the materials properties were among the ranges of our simulation, which have almost included all traditional engineering metals and a part of ceramics. Still, some interesting observations were gotten here. One of them is that when value of $\mathrm{E_L/E_T}$ is larger, the error level is relatively higher. This might due to that the influence of $\mathrm{E_L/E_T}$ on $\mathrm{P}-h$ curve is slight while compared to other three variables. It means there is a requirement of more precise forms of variable 'z' in forward equations.

Table 3-3: Summary of the errors obtained in the predictions of the indentation responses of 16 sets of transversely isotropic thin film through forward analysis functions

x (E_0/GPa)	y (σ_0/MPa)	z (E_L/E_T)	w (σ_L/σ_T)	Error of P_1 (%)	Error of P_2 (%)	Error of W_u (%)
125	300	1.25	1.15	0.08	0.94	1.06
125	300	1.45	1.15	0.09	0.85	0.89
125	300	1.25	1.35	0.65	0.42	3.78
125	300	1.45	1.35	0.42	0.49	3.53
225	300	1.25	1.15	0.67	1.36	1.71
225	300	1.45	1.15	0.43	1.29	1.81
225	300	1.25	1.35	0.09	0.67	4.42
225	300	1.45	1.35	0.16	0.63	4.43
125	700	1.25	1.15	0.27	0.29	0.65
125	700	1.45	1.15	0.44	0.17	0.66
125	700	1.25	1.35	0.81	1.06	1.17
125	700	1.45	1.35	0.79	1.05	1.47
225	700	1.25	1.15	0.31	0.74	0.32
225	700	1.45	1.15	0.13	0.37	0.35
225	700	1.25	1.35	0.65	0.24	0.44
225	700	1.45	1.35	0.77	0.27	0.78

4 Conclusions and prospects

Since, there are lots of engineering 'bulk' and 'thin film' materials exhibit transversely isotropic properties, it's important to establish a deeper understanding of their mechanic properties and behaviors, together to create a powerful tool to analysis them. Prior studies were largely focused on the understanding of the relationship between indenter displacement h and the force worked on it, as P, and as well developing forward analysis equations for future predictions. The main methods applied here are dimensional analysis method and infinite element method. Main conclusions from present study are highlighted as follows:

(a) Exponent m of $\mathrm{P}-\mathrm{h}$ curve varies when displacement h increase for transversely isotropic thin film instrument indentation. If the film is 'softer' than the substrate, m intend to increase first, and then drop to two; while if the film is 'hard', exponent would decrease at the beginning, then grow up to two.

(b) By constructing a large database of 630 sets of materials properties, the effects of different variables on characteristic parameters were researched. For example, σ_0/σ_S makes all three parameters increase, $\mathrm{E_L/E_T}$ makes total three parameters decrease, while $\mathrm{E_0/E_S}$ makes $\mathrm{P_1}$ and $\mathrm{P_1}$ grow, but let $\mathrm{W_u}$ down.

(c) A maximum of 4% mismatch was found between the result of FEM and those predicted by forward analysis functions. And almost all high level of errors appeared when the value of $\mathrm{E_L/E_T}$ is large. This might due to that $\mathrm{E_L/E_T}$ can only affect $\mathrm{P}-\mathrm{h}$ curve slightly, so there is a requirement of more precise forms of variable 'z' in forward equations.

This thesis just laid a foundation for the investigation of researching transversely isotropic thin film on a substrate with already known properties. In order to further understand the relationships between $\mathrm{P}-\mathrm{h}$ curve and thin film properties, reverse analysis are suggested. Also, we will include the influence of strain hardening constant in our future work. And indentation alone transverse direction is always on our list.

Moreover, due to that the uniqueness of reverse analysis is still unknown, so a more powerful analysis strategy is expected to show up.

5 Reference

1. Oliver, W.C. and G.M. Pharr, *Nanoindentation in materials research: Past, present, and future.* Mrs Bulletin, 2010. **35**(11): p. 897-907.
2. Venkatesh, T.A., et al., *Determination of elasto-plastic properties by instrumented sharp indentation: Guidelines for property extraction.* Scripta Materialia, 2000. **42**(9): p. 833-839.
3. Lan, H.Z. and T.A. Venkatesh, *On the sensitivity characteristics in the determination of the elastic and plastic properties of materials through multiple indentation.* Journal of Materials Research, 2007. **22**(4): p. 1043-1063.
4. Oliver, W.C. and G.M. Pharr, *An Improved Technique for Determining Hardness and Elastic-Modulus Using Load and Displacement Sensing Indentation Experiments.* Journal of Materials Research, 1992. **7**(6): p. 1564-1583.
5. Sneddon, I.N., *The relation between load and penetration in the axisymmetric Boussinesq problem for a punch of arbitrary profile.* International Journal of Engineering Science, 1965. **3**(1): p. 47-57.
6. Oliver, W.C. and G.M. Pharr, *Measurement of hardness and elastic modulus by instrumented indentation: Advances in understanding and refinements to methodology.* Journal of Materials Research, 2004. **19**(1): p. 3-20.
7. Bolshakov, A. and G.M. Pharr, *Influences of pileup on the measurement of mechanical properties by load and depth sensing indentation techniques.* Journal of Materials Research, 1998. **13**(4): p. 1049-1058.
8. Dao, M., et al., *Computational modeling of the forward and reverse problems in instrumented sharp indentation.* Acta Materialia, 2001. **49**(19): p. 3899-3918.
9. Cheng, Y.T. and C.M. Cheng, *Scaling approach to conical indentation in elastic-plastic solids with work hardening.* Journal of Applied Physics, 1998. **84**(3): p. 1284-1291.
10. Cheng, Y.T. and C.M. Cheng, *Relationships between hardness, elastic modulus, and the work of indentation.* Applied Physics Letters, 1998. **73**(5): p. 614-616.
11. Verdier §, M., et al., *Microstructure, indentation and work hardening of Cu/Ag multilayers.* Philosophical Magazine, 2006. **86**(32): p. 5009-5016.
12. Suresh, S. and A.E. Giannakopoulos, *A new method for estimating residual stresses by instrumented sharp indentation.* Acta Materialia, 1998. **46**(16): p. 5755-5767.
13. Deng, X., et al., *Deformation behavior of (Cu, Ag)–Sn intermetallics by nanoindentation.* Acta materialia, 2004. **52**(14): p. 4291-4303.
14. Deng, X., et al., *Mechanical Behavior of Multilayered Nanoscale Metal‐Ceramic Composites.* Advanced Engineering Materials, 2005. **7**(12): p. 1099-1108.
15. Barshilia, H.C. and K. Rajam, *Characterization of Cu/Ni multilayer coatings by nanoindentation and atomic force microscopy.* Surface and Coatings Technology, 2002. **155**(2): p. 195-202.
16. Carvalho, N. and J.T.M. De Hosson, *Deformation mechanisms in TiN/(Ti, Al) N multilayers under depth-sensing indentation.* Acta materialia, 2006. **54**(7): p. 1857-1862.
17. Wen, S., et al., *Indentation creep behavior of nano-scale Ag/Co multilayers.* Scripta materialia, 2006. **55**(2): p. 187-190.
18. Zhao, B., B. Xu, and Z. Yue, *Indentation creep-fatigue test on aluminum alloy 2A12.* Materials Science and Engineering: A, 2010. **527**(16): p. 4519-4522.
19. Goldsby, D.L., et al., *Nanoindentation creep of quartz, with implications for rate- and state-variable friction laws relevant to earthquake mechanics.* Journal of Materials Research, 2004. **19**(1): p. 357-365.

20. Ebenstein, D.M., et al., *Nanomechanical properties of calcification, fibrous tissue, and hematoma from atherosclerotic plaques.* J Biomed Mater Res A, 2009. **91**(4): p. 1028-37.
21. Yao, H., et al., *Protection mechanisms of the iron-plated armor of a deep-sea hydrothermal vent gastropod.* Proc Natl Acad Sci U S A, 2010. **107**(3): p. 987-92.
22. Nakamura, T. and Y. Gu, *Identification of elastic–plastic anisotropic parameters using instrumented indentation and inverse analysis.* Mechanics of materials, 2007. **39**(4): p. 340-356.
23. Hill, R., *A Theory of the Yielding and Plastic Flow of Anisotropic Metals.* Proceedings of the Royal Society of London Series a-Mathematical and Physical Sciences, 1948. **193**(1033): p. 281-297.
24. Cheng, Y.T. and C.M. Cheng, *Scaling, dimensional analysis, and indentation measurements.* Materials Science & Engineering R-Reports, 2004. **44**(4-5): p. 91-149.
25. Buckingham, E., *On physically similar systems, illustrations of the use of dimensional equations.* Physical Review, 1914. **4**(4): p. 345-376.
26. Wang, L.G., M. Ganor, and S.I. Rokhlin, *Inverse scaling functions in nanoindentation with sharp indenters: Determination of material properties.* Journal of Materials Research, 2005. **20**(4): p. 987-1001.
27. Zhao, M., et al., *A new approach to measure the elastic–plastic properties of bulk materials using spherical indentation.* Acta materialia, 2006. **54**(1): p. 23-32.
28. Zhao, M.H., et al., *New sharp indentation method of measuring the elastic-plastic properties of compliant and soft materials using the substrate effect.* Journal of Materials Research, 2006. **21**(12): p. 3134-3151.
29. Zhao, M., et al., *Measuring elastoplastic properties of thin films on an elastic substrate using sharp indentation.* Acta Materialia, 2007. **55**(18): p. 6260-6274.
30. Chen, X., et al., *On the uniqueness of measuring elastoplastic properties from indentation: the indistinguishable mystical materials.* Journal of the Mechanics and Physics of Solids, 2007. **55**(8): p. 1618-1660.